Mathematical Problems in Engineering

Artificial Intelligence Approaches for Energy Systems

Lead Guest Editor: Pushpendra Singh
Guest Editors: Mohan Lal Kohle and Tzung-Pei Hong

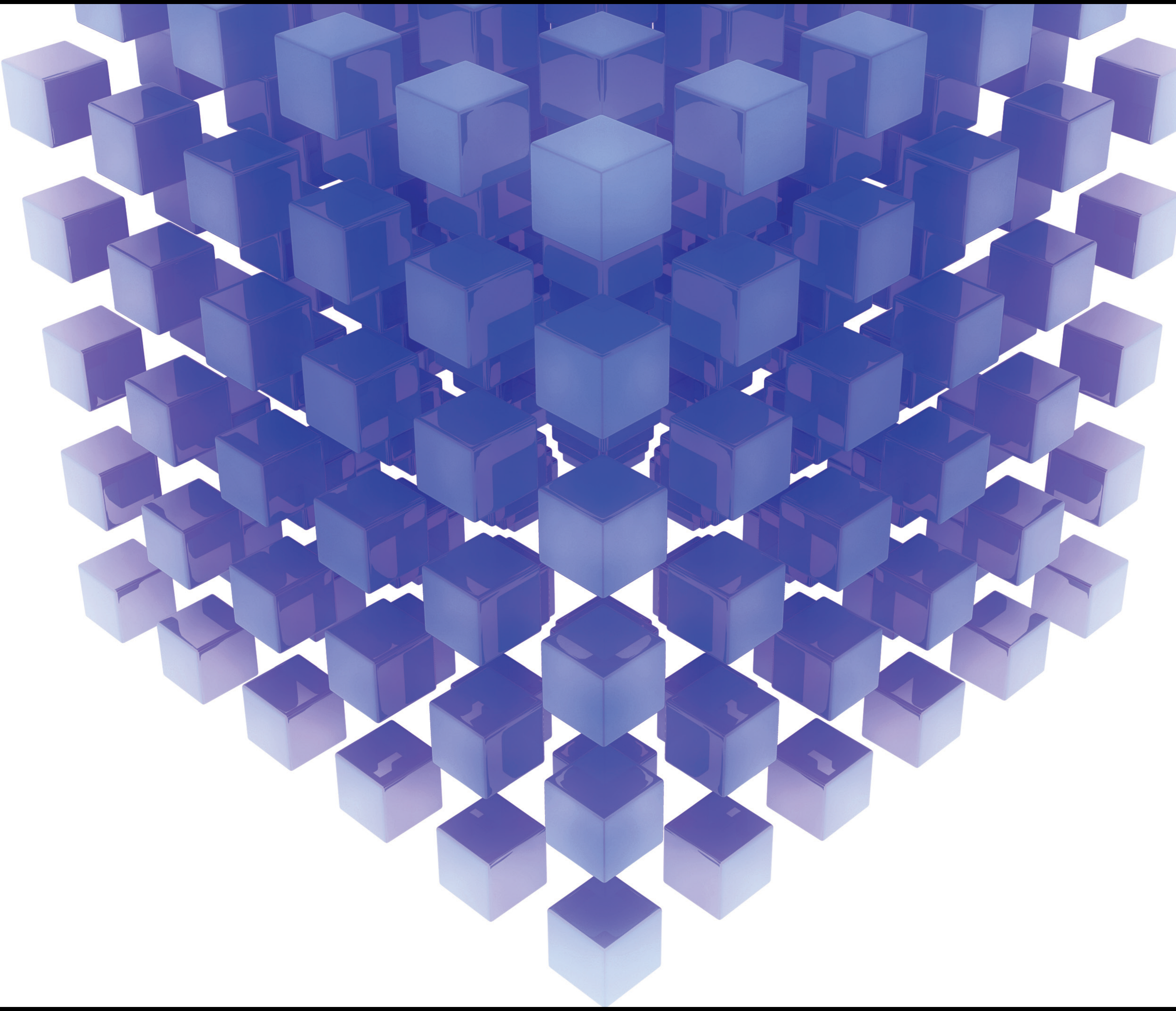

Artificial Intelligence Approaches for Energy Systems

Mathematical Problems in Engineering

Artificial Intelligence Approaches for Energy Systems

Lead Guest Editor: Pushpendra Singh
Guest Editors: Mohan Lal Kolhe and Tzung-Pei Hong

Paolo Boscariol, Italy
Daniela Boso, Italy
Guillermo Botella-Juan, Spain
Abdesselem Boulkroune, Algeria
Boulaïd Boulkroune, Belgium
Fabio Bovenga, Italy
Francesco Braghin, Italy
Ricardo Branco, Portugal
Julien Bruchon, France
Matteo Bruggi, Italy
Michele Brun, Italy
Maria Elena Bruni, Italy
Maria Angela Butturi, Italy
Bartłomiej Błachowski, Poland
Dhanamjayulu C, India
Raquel Caballero-Águila, Spain
Filippo Cacace, Italy
Salvatore Caddemi, Italy
Zuowei Cai, China
Roberto Caldelli, Italy
Francesco Cannizzaro, Italy
Maosen Cao, China
Ana Carpio, Spain
Rodrigo Carvajal, Chile
Caterina Casavola, Italy
Sara Casciati, Italy
Federica Caselli, Italy
Carmen Castillo, Spain
Inmaculada T. Castro, Spain
Miguel Castro, Portugal
Giuseppe Catalanotti, United Kingdom
Alberto Cavallo, Italy
Gabriele Cazzulani, Italy
Fatih Vehbi Celebi, Turkey
Miguel Cerrolaza, Venezuela
Gregory Chagnon, France
Ching-Ter Chang, Taiwan
Kuei-Lun Chang, Taiwan
Qing Chang, USA
Xiaoheng Chang, China
Prasenjit Chatterjee, Lithuania
Kacem Chehdi, France
Peter N. Cheimets, USA
Chih-Chiang Chen, Taiwan
He Chen, China
Kebing Chen, China
Mengxin Chen, China
Shyi-Ming Chen, Taiwan
Xizhong Chen, Ireland
Xue-Bo Chen, China
Zhiwen Chen, China
Qiang Cheng, USA
Zeyang Cheng, China
Luca Chiapponi, Italy
Francisco Chicano, Spain
Tirivanhu Chinyoka, South Africa
Adrian Chmielewski, Poland
Seongim Choi, USA
Gautam Choubey, India
Hung-Yuan Chung, Taiwan
Yusheng Ci, China
Simone Cinquemani, Italy
Roberto G. Citarella, Italy
Joaquim Ciurana, Spain
John D. Clayton, USA
Piero Colajanni, Italy
Giuseppina Colicchio, Italy
Vassilios Constantoudis, Greece
Enrico Conte, Italy
Alessandro Contento, USA
Mario Cools, Belgium
Gino Cortellessa, Italy
Carlo Cosentino, Italy
Paolo Crippa, Italy
Erik Cuevas, Mexico
Guozeng Cui, China
Mehmet Cunkas, Turkey
Giuseppe D'Aniello, Italy
Peter Dabnichki, Australia
Weizhong Dai, USA
Zhifeng Dai, China
Purushothaman Damodaran, USA
Sergey Dashkovskiy, Germany
Adiel T. De Almeida-Filho, Brazil
Fabio De Angelis, Italy
Samuele De Bartolo, Italy
Stefano De Miranda, Italy
Filippo De Monte, Italy

Antoine Grall, France
George A. Gravvanis, Greece
Fabrizio Greco, Italy
David Greiner, Spain
Jason Gu, Canada
Federico Guarracino, Italy
Michele Guida, Italy
Muhammet Gul, Turkey
Dong-Sheng Guo, China
Hu Guo, China
Zhaoxia Guo, China
Yusuf Gurefe, Turkey
Salim HEDDAM, Algeria
ABID HUSSANAN, China
Quang Phuc Ha, Australia
Li Haitao, China
Petr Hájek, Czech Republic
Mohamed Hamdy, Egypt
Muhammad Hamid, United Kingdom
Renke Han, United Kingdom
Weimin Han, USA
Xingsi Han, China
Zhen-Lai Han, China
Thomas Hanne, Switzerland
Xinan Hao, China
Mohammad A. Hariri-Ardebili, USA
Khalid Hattaf, Morocco
Defeng He, China
Xiao-Qiao He, China
Yanchao He, China
Yu-Ling He, China
Ramdane Hedjar, Saudi Arabia
Jude Hemanth, India
Reza Hemmati, Iran
Nicolae Herisanu, Romania
Alfredo G. Hernández-Diaz, Spain
M.I. Herreros, Spain
Eckhard Hitzer, Japan
Paul Honeine, France
Jaromir Horacek, Czech Republic
Lei Hou, China
Yingkun Hou, China
Yu-Chen Hu, Taiwan
Yunfeng Hu, China
Can Huang, China
Gordon Huang, Canada
Linsheng Huo, China
Sajid Hussain, Canada
Asier Ibeas, Spain
Orest V. Iftime, The Netherlands
Przemyslaw Ignaciuk, Poland
Giacomo Innocenti, Italy
Emilio Insfran Pelozo, Spain
Azeem Irshad, Pakistan
Alessio Ishizaka, France
Benjamin Ivorra, Spain
Breno Jacob, Brazil
Reema Jain, India
Tushar Jain, India
Amin Jajarmi, Iran
Chiranjibe Jana, India
Łukasz Jankowski, Poland
Samuel N. Jator, USA
Juan Carlos Jáuregui-Correa, Mexico
Kandasamy Jayakrishna, India
Reza Jazar, Australia
Khalide Jbilou, France
Isabel S. Jesus, Portugal
Chao Ji, China
Qing-Chao Jiang, China
Peng-fei Jiao, China
Ricardo Fabricio Escobar Jiménez, Mexico
Emilio Jiménez Macías, Spain
Maolin Jin, Republic of Korea
Zhuo Jin, Australia
Ramash Kumar K, India
BHABEN KALITA, USA
MOHAMMAD REZA KHEDMATI, Iran
Viacheslav Kalashnikov, Mexico
Mathiyalagan Kalidass, India
Tamas Kalmar-Nagy, Hungary
Rajesh Kaluri, India
Jyotheeswara Reddy Kalvakurthi, India
Zhao Kang, China
Ramani Kannan, Malaysia
Tomasz Kapitaniak, Poland
Julius Kaplunov, United Kingdom
Konstantinos Karamanos, Belgium
Michal Kawulok, Poland

Irfan Kaymaz, Turkey
Vahid Kayvanfar, Qatar
Krzysztof Kecik, Poland
Mohamed Khader, Egypt
Chaudry M. Khalique, South Africa
Mukhtaj Khan, Pakistan
Shahid Khan, Pakistan
Nam-Il Kim, Republic of Korea
Philipp V. Kiryukhantsev-Korneev, Russia
P.V.V Kishore, India
Jan Koci, Czech Republic
Ioannis Kostavelis, Greece
Sotiris B. Kotsiantis, Greece
Frederic Kratz, France
Vamsi Krishna, India
Edyta Kucharska, Poland
Krzysztof S. Kulpa, Poland
Kamal Kumar, India
Prof. Ashwani Kumar, India
Michal Kunicki, Poland
Cedrick A. K. Kwuimy, USA
Kyandoghere Kyamakya, Austria
Ivan Kyrchei, Ukraine
Márcio J. Lacerda, Brazil
Eduardo Lalla, The Netherlands
Giovanni Lancioni, Italy
Jaroslaw Latalski, Poland
Hervé Laurent, France
Agostino Lauria, Italy
Aimé Lay-Ekuakille, Italy
Nicolas J. Leconte, France
Kun-Chou Lee, Taiwan
Dimitri Lefebvre, France
Eric Lefevre, France
Marek Lefik, Poland
Yaguo Lei, China
Kauko Leiviskä, Finland
Ervin Lenzi, Brazil
ChenFeng Li, China
Jian Li, USA
Jun Li, China
Yueyang Li, China
Zhao Li, China
Zhen Li, China
En-Qiang Lin, USA
Jian Lin, China
Qibin Lin, China
Yao-Jin Lin, China
Zhiyun Lin, China
Bin Liu, China
Bo Liu, China
Heng Liu, China
Jianxu Liu, Thailand
Lei Liu, China
Sixin Liu, China
Wanquan Liu, China
Yu Liu, China
Yuanchang Liu, United Kingdom
Bonifacio Llamazares, Spain
Alessandro Lo Schiavo, Italy
Jean Jacques Loiseau, France
Francesco Lolli, Italy
Paolo Lonetti, Italy
António M. Lopes, Portugal
Sebastian López, Spain
Luis M. López-Ochoa, Spain
Vassilios C. Loukopoulos, Greece
Gabriele Maria Lozito, Italy
Zhiguo Luo, China
Gabriel Luque, Spain
Valentin Lychagin, Norway
YUE MEI, China
Junwei Ma, China
Xuanlong Ma, China
Antonio Madeo, Italy
Alessandro Magnani, Belgium
Toqeer Mahmood, Pakistan
Fazal M. Mahomed, South Africa
Arunava Majumder, India
Sarfraz Nawaz Malik, Pakistan
Paolo Manfredi, Italy
Adnan Maqsood, Pakistan
Muazzam Maqsood, Pakistan
Giuseppe Carlo Marano, Italy
Damijan Markovic, France
Filipe J. Marques, Portugal
Luca Martinelli, Italy
Denizar Cruz Martins, Brazil

Francisco J. Martos, Spain
Elio Masciari, Italy
Paolo Massioni, France
Alessandro Mauro, Italy
Jonathan Mayo-Maldonado, Mexico
Pier Luigi Mazzeo, Italy
Laura Mazzola, Italy
Driss Mehdi, France
Zahid Mehmood, Pakistan
Roderick Melnik, Canada
Xiangyu Meng, USA
Jose Merodio, Spain
Alessio Merola, Italy
Mahmoud Mesbah, Iran
Luciano Mescia, Italy
Laurent Mevel, France
Constantine Michailides, Cyprus
Mariusz Michta, Poland
Prankul Middha, Norway
Aki Mikkola, Finland
Giovanni Minafò, Italy
Edmondo Minisci, United Kingdom
Hiroyuki Mino, Japan
Dimitrios Mitsotakis, New Zealand
Ardashir Mohammadzadeh, Iran
Francisco J. Montáns, Spain
Francesco Montefusco, Italy
Gisele Mophou, France
Rafael Morales, Spain
Marco Morandini, Italy
Javier Moreno-Valenzuela, Mexico
Simone Morganti, Italy
Caroline Mota, Brazil
Aziz Moukrim, France
Shen Mouquan, China
Dimitris Mourtzis, Greece
Emiliano Mucchi, Italy
Taseer Muhammad, Saudi Arabia
Ghulam Muhiuddin, Saudi Arabia
Amitava Mukherjee, India
Josefa Mula, Spain
Jose J. Muñoz, Spain
Giuseppe Muscolino, Italy
Marco Mussetta, Italy
Hariharan Muthusamy, India
Alessandro Naddeo, Italy
Raj Nandkeolyar, India
Keivan Navaie, United Kingdom
Soumya Nayak, India
Adrian Neagu, USA
Erivelton Geraldo Nepomuceno, Brazil
AMA Neves, Portugal
Ha Quang Thinh Ngo, Vietnam
Nhon Nguyen-Thanh, Singapore
Papakostas Nikolaos, Ireland
Jelena Nikolic, Serbia
Tatsushi Nishi, Japan
Shanzhou Niu, China
Ben T. Nohara, Japan
Mohammed Nouari, France
Mustapha Nourelfath, Canada
Kazem Nouri, Iran
Ciro Núñez-Gutiérrez, Mexico
Wlodzimierz Ogryczak, Poland
Roger Ohayon, France
Krzysztof Okarma, Poland
Mitsuhiro Okayasu, Japan
Murat Olgun, Turkey
Diego Oliva, Mexico
Alberto Olivares, Spain
Enrique Onieva, Spain
Calogero Orlando, Italy
Susana Ortega-Cisneros, Mexico
Sergio Ortobelli, Italy
Naohisa Otsuka, Japan
Sid Ahmed Ould Ahmed Mahmoud, Saudi Arabia
Taoreed Owolabi, Nigeria
EUGENIA PETROPOULOU, Greece
Arturo Pagano, Italy
Madhumangal Pal, India
Pasquale Palumbo, Italy
Dragan Pamučar, Serbia
Weifeng Pan, China
Chandan Pandey, India
Rui Pang, United Kingdom
Jürgen Pannek, Germany
Elena Panteley, France
Achille Paolone, Italy

George A. Papakostas, Greece
Xosé M. Pardo, Spain
You-Jin Park, Taiwan
Manuel Pastor, Spain
Pubudu N. Pathirana, Australia
Surajit Kumar Paul, India
Luis Payá, Spain
Igor Pažanin, Croatia
Libor Pekař, Czech Republic
Francesco Pellicano, Italy
Marcello Pellicciari, Italy
Jian Peng, China
Mingshu Peng, China
Xiang Peng, China
Xindong Peng, China
Yuexing Peng, China
Marzio Pennisi, Italy
Maria Patrizia Pera, Italy
Matjaz Perc, Slovenia
A. M. Bastos Pereira, Portugal
Wesley Peres, Brazil
F. Javier Pérez-Pinal, Mexico
Michele Perrella, Italy
Francesco Pesavento, Italy
Francesco Petrini, Italy
Hoang Vu Phan, Republic of Korea
Lukasz Pieczonka, Poland
Dario Piga, Switzerland
Marco Pizzarelli, Italy
Javier Plaza, Spain
Goutam Pohit, India
Dragan Poljak, Croatia
Jorge Pomares, Spain
Hiram Ponce, Mexico
Sébastien Poncet, Canada
Volodymyr Ponomaryov, Mexico
Jean-Christophe Ponsart, France
Mauro Pontani, Italy
Sivakumar Poruran, India
Francesc Pozo, Spain
Aditya Rio Prabowo, Indonesia
Anchasa Pramuanjaroenkij, Thailand
Leonardo Primavera, Italy
B Rajanarayan Prusty, India
Krzysztof Puszynski, Poland
Chuan Qin, China
Dongdong Qin, China
Jianlong Qiu, China
Giuseppe Quaranta, Italy
DR. RITU RAJ, India
Vitomir Racic, Italy
Carlo Rainieri, Italy
Kumbakonam Ramamani Rajagopal, USA
Ali Ramazani, USA
Angel Manuel Ramos, Spain
Higinio Ramos, Spain
Muhammad Afzal Rana, Pakistan
Muhammad Rashid, Saudi Arabia
Manoj Rastogi, India
Alessandro Rasulo, Italy
S.S. Ravindran, USA
Abdolrahman Razani, Iran
Alessandro Reali, Italy
Jose A. Reinoso, Spain
Oscar Reinoso, Spain
Haijun Ren, China
Carlo Renno, Italy
Fabrizio Renno, Italy
Shahram Rezapour, Iran
Ricardo Riaza, Spain
Francesco Riganti-Fulginei, Italy
Gerasimos Rigatos, Greece
Francesco Ripamonti, Italy
Jorge Rivera, Mexico
Eugenio Roanes-Lozano, Spain
Ana Maria A. C. Rocha, Portugal
Luigi Rodino, Italy
Francisco Rodríguez, Spain
Rosana Rodríguez López, Spain
Francisco Rossomando, Argentina
Jose de Jesus Rubio, Mexico
Weiguo Rui, China
Rubén Ruiz, Spain
Ivan D. Rukhlenko, Australia
Dr. Eswaramoorthi S., India
Weichao SHI, United Kingdom
Chaman Lal Sabharwal, USA
Andrés Sáez, Spain

Bekir Sahin, Turkey
Laxminarayan Sahoo, India
John S. Sakellariou, Greece
Michael Sakellariou, Greece
Salvatore Salamone, USA
Jose Vicente Salcedo, Spain
Alejandro Salcido, Mexico
Alejandro Salcido, Mexico
Nunzio Salerno, Italy
Rohit Salgotra, India
Miguel A. Salido, Spain
Sinan Salih, Iraq
Alessandro Salvini, Italy
Abdus Samad, India
Sovan Samanta, India
Nikolaos Samaras, Greece
Ramon Sancibrian, Spain
Giuseppe Sanfilippo, Italy
Omar-Jacobo Santos, Mexico
J Santos-Reyes, Mexico
José A. Sanz-Herrera, Spain
Musavarah Sarwar, Pakistan
Shahzad Sarwar, Saudi Arabia
Marcelo A. Savi, Brazil
Andrey V. Savkin, Australia
Tadeusz Sawik, Poland
Roberta Sburlati, Italy
Gustavo Scaglia, Argentina
Thomas Schuster, Germany
Hamid M. Sedighi, Iran
Mijanur Rahaman Seikh, India
Tapan Senapati, China
Lotfi Senhadji, France
Junwon Seo, USA
Michele Serpilli, Italy
Silvestar Šesnić, Croatia
Gerardo Severino, Italy
Ruben Sevilla, United Kingdom
Stefano Sfarra, Italy
Dr. Ismail Shah, Pakistan
Leonid Shaikhet, Israel
Vimal Shanmuganathan, India
Prayas Sharma, India
Bo Shen, Germany
Hang Shen, China
Xin Pu Shen, China
Dimitri O. Shepelsky, Ukraine
Jian Shi, China
Amin Shokrollahi, Australia
Suzanne M. Shontz, USA
Babak Shotorban, USA
Zhan Shu, Canada
Angelo Sifaleras, Greece
Nuno Simões, Portugal
Mehakpreet Singh, Ireland
Piyush Pratap Singh, India
Rajiv Singh, India
Seralathan Sivamani, India
S. Sivasankaran, Malaysia
Christos H. Skiadas, Greece
Konstantina Skouri, Greece
Neale R. Smith, Mexico
Bogdan Smolka, Poland
Delfim Soares Jr., Brazil
Alba Sofi, Italy
Francesco Soldovieri, Italy
Raffaele Solimene, Italy
Yang Song, Norway
Jussi Sopanen, Finland
Marco Spadini, Italy
Paolo Spagnolo, Italy
Ruben Specogna, Italy
Vasilios Spitas, Greece
Ivanka Stamova, USA
Rafał Stanisławski, Poland
Miladin Stefanović, Serbia
Salvatore Strano, Italy
Yakov Strelniker, Israel
Kangkang Sun, China
Qiuqin Sun, China
Shuaishuai Sun, Australia
Yanchao Sun, China
Zong-Yao Sun, China
Kumarasamy Suresh, India
Sergey A. Suslov, Australia
D.L. Suthar, Ethiopia
D.L. Suthar, Ethiopia
Andrzej Swierniak, Poland
Andras Szekrenyes, Hungary
Kumar K. Tamma, USA

Yong (Aaron) Tan, United Kingdom
Marco Antonio Taneco-Hernández, Mexico
Lu Tang, China
Tianyou Tao, China
Hafez Tari, USA
Alessandro Tasora, Italy
Sergio Teggi, Italy
Adriana del Carmen Téllez-Anguiano, Mexico
Ana C. Teodoro, Portugal
Efstathios E. Theotokoglou, Greece
Jing-Feng Tian, China
Alexander Timokha, Norway
Stefania Tomasiello, Italy
Gisella Tomasini, Italy
Isabella Torcicollo, Italy
Francesco Tornabene, Italy
Mariano Torrisi, Italy
Thang nguyen Trung, Vietnam
George Tsiatas, Greece
Le Anh Tuan, Vietnam
Nerio Tullini, Italy
Emilio Turco, Italy
Ilhan Tuzcu, USA
Efstratios Tzirtzilakis, Greece
FRANCISCO UREÑA, Spain
Filippo Ubertini, Italy
Mohammad Uddin, Australia
Mohammad Safi Ullah, Bangladesh
Serdar Ulubeyli, Turkey
Mati Ur Rahman, Pakistan
Panayiotis Vafeas, Greece
Giuseppe Vairo, Italy
Jesus Valdez-Resendiz, Mexico
Eusebio Valero, Spain
Stefano Valvano, Italy
Carlos-Renato Vázquez, Mexico
Martin Velasco Villa, Mexico
Franck J. Vernerey, USA
Georgios Veronis, USA
Vincenzo Vespri, Italy
Renato Vidoni, Italy
Venkatesh Vijayaraghavan, Australia
Anna Vila, Spain
Francisco R. Villatoro, Spain
Francesca Vipiana, Italy
Stanislav Vítek, Czech Republic
Jan Vorel, Czech Republic
Michael Vynnycky, Sweden
Mohammad W. Alomari, Jordan
Roman Wan-Wendner, Austria
Bingchang Wang, China
C. H. Wang, Taiwan
Dagang Wang, China
Guoqiang Wang, China
Huaiyu Wang, China
Hui Wang, China
J.G. Wang, China
Ji Wang, China
Kang-Jia Wang, China
Lei Wang, China
Qiang Wang, China
Qingling Wang, China
Weiwei Wang, China
Xinyu Wang, China
Yong Wang, China
Yung-Chung Wang, Taiwan
Zhenbo Wang, USA
Zhibo Wang, China
Waldemar T. Wójcik, Poland
Chi Wu, Australia
Qiuhong Wu, China
Yuqiang Wu, China
Zhibin Wu, China
Zhizheng Wu, China
Michalis Xenos, Greece
Hao Xiao, China
Xiao Ping Xie, China
Qingzheng Xu, China
Binghan Xue, China
Yi Xue, China
Joseph J. Yame, France
Chuanliang Yan, China
Xinggang Yan, United Kingdom
Hongtai Yang, China
Jixiang Yang, China
Mijia Yang, USA
Ray-Yeng Yang, Taiwan

Contents

Hindawi
Mathematical Problems in Engineering
Volume 2021, Article ID 3577087, 14 pages
https://doi.org/10.1155/2021/3577087

Research Article

Multiarea Economic Dispatch Using Evolutionary Algorithms

Sanjay Kumar,[1] **Vineet Kumar**,[2] **Nitish Katal**,[3] **Sanjay Kumar Singh**,[4] **Sumit Sharma**,[2] **and Pushpendra Singh**[5]

[1]*Department of Electrical Engineering, UIT, Himachal Pradesh University, Shimla, H.P, India*
[2]*Department of Electrical Engineering, National Institute of Technology, Hamirpur, H.P, India*
[3]*School of Electronics, Indian Institute of Information Technology, Una, H.P, India*
[4]*Department of Electrical & Electronics Engineering, Amity University Rajasthan, Jaipur, India*
[5]*Department of Electrical & Electronics Engineering, JK Lakshmipat University, Jaipur, Rajasthan, India*

Correspondence should be addressed to Sanjay Kumar; sanjnitham@gmail.com

Received 5 April 2021; Revised 1 July 2021; Accepted 17 August 2021; Published 1 September 2021

Academic Editor: Tzung-Pei Hong

Multiarea economic dispatch (MAED) is a vital problem in the present power system to allocate the power generation through dispatch strategies to minimize fuel cost. In economic dispatch, this power generation distribution always needs to satisfy the following constraints: generating limit, transmission line, and power balance. MAED is a complex and nonlinear problem and cannot be solved with classical techniques. Many metaheuristic methods have been used to solve economic dispatch problems. In this study, the dynamic particle swarm optimization (DPSO) and grey wolf optimizer (GWO) have been used to solve the MAED problem for single-area 3 generation units, a two-area system with four generating units, and four areas with 40-unit system. The hunting and social behaviors of grey wolves are implemented to obtain optimal results. During the optimization search, this algorithm does not require any information regarding the objective function's gradient. The tunable parameters of the original PSO that are three parameters are dynamically controlled in this work that provides the efficient cost values in less execution time although satisfying all the MAED problem's diverse constraints. In this study, the authors also implemented the GWO algorithm with two tunable parameters, and its execution is straightforward to implement for the MAED problem.

1. Introduction

The application of economic dispatch (ED) in the operation of the modern power system has a great significance. System demand is economically allocated between different multiarea generators by considering all constraints [1]. ED for multiple areas has paid limited attention. Large and small utilities have many constraints to transmit power through tie lines. All utilities and power pools have different generation characteristics and load patterns in modern power sectors, including spinning reserves. Therefore, the main objective of ED is to minimize the fuel cost of all the generators and satisfy all the constraints such as power balance, losses, and generation limits. In the deregulated environment, the generator with the lowest cost should operate with its maximum capacity and transmit more power to those areas consisting of more expensive generating units. MAED is a form of ED model that satisfies multiple constraints simultaneously. In this study, the significance of power balance, generation limits, and transmission line constraints in the optimal scheduling of power generation has been considered.

Previous ED problem was solved by lambda-iteration method, gradient method, reduced gradient method, NR method, and other methods, such as participation factor method and binary-weighted method [1]. However, these methods required considerable computation effort to solve the ED problem. In multiareas, large interconnected power system ED problem becomes more complex with different cost characteristics. Therefore, to overcome these shortcomings, metaheuristics methodologies can be used. Many such methods were implemented in ED by various researchers. In this respect, evolutionary algorithms, such as simulated annealing (SA) [2], genetic algorithm (GA) [3], evolutionary programming (EP) [4], artificial neural network (ANN) [5], ant colony optimization (ACO) [6], particle swarm optimization (PSO) [7], artificial immune system (AIS) [8], differential evolution (DE) [9], bacterial foraging algorithm (BFA) [10], and biogeography-based optimization (BBO) [11], have been successfully applied to have complex ED problem without any limitation in size and condition of cost curves. Shoults et al. [12] have made ED by considering import and export constraints for the single-area and three-area problems. Yalcinoz and Short [13] have considered transmission constraints for two areas' power systems and applied the ANN approach for the ED problem. Seiffert [14] has used linear programming methodologies. The author calculated the incremental cost for each area, and according to total cost power, cost and tie line values were adjusted. The problem with this method was not feasible on large interconnected power systems. Chen and Chen [15] have used the direct space method to solve MAED problems. The author built an MAGS algorithm to establish a relation between dependability and system security. The power system of Taiwan has been selected for this work by the author. Manoharan et al. [16] have applied the evaluation algorithm (EA) and Karush–Kuhn–Tucker (KKT) conditions based on optimal confirmation to the MAED problem. KKT-trained variables have been applied to the results obtained by EAs to check optimality. The obtained results using the KKT criterion were compared with linear programming (LP) and dynamic programming (DP) results. The authors concluded that this technique provides better CPU time and standard deviation. Sharma et al. [17] presented differential evolution with a time-varying mutation technique to solve MAED by considering tie line capacity constraints. Venkatakrishnan et al. [18] applied the GWO method to solve the ED problems by considering thermal valves. Evolutionary-based optimization methods are becoming more popular for ED problems due to their advantages, such as the absence of convexity assumptions, better search capability, and simplicity. Many such methods reported in the literature are neural network (NN), tabu search (TS), simulating annealing (SA) [2], particle swarm optimization [7], genetic algorithm (GA) [3], harmony search (HS) [16], ant colony optimization (ACO) [16], and differential evolution (DE) [19]. Some researchers have proposed comprehensive reviews of metaheuristic optimization methods to solve ED problems. These reviews suggested that PSO and DE techniques are more popular for solving ED problems due to their simplicity, fast convergence rate, greater flexibility to search optimum global points, and easy implementation.

However, all evolutionary techniques required a suitable balance between global search (GS) and local search (LS). Few researchers have focused on convergence time, optimal parameters tuning, premature convergence, and so on. Researchers have attempted to handle these issues using various strategies, such as modified evolutionary techniques [20] and hybridization of algorithms [21, 22]. Jain and Pandit [23] have implemented the PSO technique to solve the MAED problem. The authors have modified the PSO technique for the general search to avoid premature convergence. However, AI techniques are becoming popular for nonconvex, multimodal, discontinuous optimization problems for which traditional methods cannot provide a solution. Manoharan et al. [16] have applied EP with the LMO approach to solving the ED problem. The authors reported that the EP-LMO approach has better accuracy and convergence rate than EP. This study focuses on applying DPSO and GWO with optimal mutation to provide an accurate and feasible solution for the ED problems. The main drawback of classical approaches is knocking at local optima and may not offer the best solution. Second, all classical methods are based on the assumption that their objective function to be handled is continuous and differentiable, whereas the practical power system is more complex. Contemporary intelligent techniques have the advantage of being versatile in handling qualitative constraints. Still, their main drawback is that the computational time increases exponentially as the size of the problem increases, and time to convergence is uncertain (convergences are guaranteed). Metaheuristics approaches have been applied to overcome these shortcomings.

Apart from aforementioned papers, there are also some recent studies on multiarea economic dispatch problems, which are hybridization of differential evolution (DE) with immunized ant colony optimization (ACO) [24], electro search optimization approach (ESOA) [25, 26], uncertainty of MAED problem using Monte Carlo simulation [27], water wave optimization (WWO) [28], krill herd algorithm (KHA) [29], dynamic dispatch in wind-based power system using chaotic grasshopper optimization algorithm (CGOA) [30], hybridization of chaotic particle swarm optimization (CPSO) and genetic algorithm (GA) is (HCPSOGA) [31], squirrel search optimization (SSO) [32], complete review of metaheuristics on MAED problem [33], salp swarm algorithm (SSA) on stochastic nature of wind [34], improved grasshopper optimization algorithm (GOA) [35], Coulomb's and Franklin's law-based optimizer [36], fast convergence evolutionary programming (FCEP) [37], artificial bee colony (ABC) [38], nature-inspired optimization (NIO) [39], and hybridization of shuffled frog leaping algorithm with PSO considering emissions on MAED problems [40].

The study also compares the solution obtained using the PSO and GWO method to find the appropriate application and accuracy of these techniques. According to the authors' knowledge, proposed DPSO with all variants of PSO and GWO techniques have not been applied yet by considering valve point loading on these test systems.

2. Problem Formulation

The objective function is to minimize the total fuel cost of generation between all interconnected areas by considering all the constraints. Valve point loading (VPL) directly affects the objective function and produces distortion in heat rate characteristics in ED problems. The introduction of VPL results in the objective function nonconvex, discontinuous, and result in multiple minima of the cost function. Therefore, in the present objective part, the VPL is modeled as a sinusoidal function [38] in the input-output cost function to rectify the effect of VPL, and it is given as

$$\min F\left(P_{Gij}\right) = \sum_{i=1}^{M}\sum_{j=1}^{N_{Gi}}\left(a_{ij} + b_{ij}P_{Gij} + c_{ij}P_{Gij}^{2}\right) + \left|e_{ij}\sin\left(f_{ij}\left(P_{Gij}^{\min} - P_{Gij}\right)\right)\right|, \tag{1}$$

where P_{Gij} is the power generation of ith to jth units; a_{ij}, b_{ij}, and c_{ij} are the fuel cost coefficients; and e_{ij} and f_{ij} are the fuel cost coefficients of the ith to jth units of the VPL model.

Tie line power flow between areas plays a significant role in deciding the operating cost in multiarea power systems. Taking into consideration the cost of transmission through each tie line, the objective function of MAED is given in the following equation.

The objective function of MAED is stated as follows:

Constraints:

Area power balance: the maximum power generation through all available generators is equal to the demand P_{Di}. In ED, the area power balance constraints, each area power should meet with generation.

$$\sum_{j=1}^{N_{Gi}} P_{Gij} = P_{Di} + \sum_{m,i\neq m} P_{Tim}, \quad i \in \{1, 2, \ldots, M\}. \tag{2}$$

Generator constraints: in generating limit constraint, the output of each unit should satisfy the upper and lower limits of generations.

$$P_{Gij}^{\min} \le P_{Gij} \le P_{Gij}^{\max}. \tag{3}$$

Tie line constraints: the flows through tie line should also be in the maximum and minimum limit range. These limits of power flow are important and are stated as follows:

$$\begin{aligned} P_{T\min} \le P_{Tm,j} \le P_{T\max}, \quad m = 1, 2, \ldots, M, j = 1, 2, \ldots, M, j \neq m, \\ P_{T\min} \le P_{Tj,m} \le P_{T\max}, \quad m = 1, 2, \ldots, M, j = 1, 2, \ldots, M, j \neq m. \end{aligned} \tag{4}$$

3. Solution Technique

In the modern era, the computer-aided application in power systems has been increased. The application of evolutionary soft computing techniques in power systems has become more popular for solving optimization problems. The popularity of these techniques in complex power systems is increased due to their ease of implementation and reliable operation. Moreover, the modern interconnected power system has mixed types, that is, highly nonlinear cost characteristics functions. Solving these mixed-type functions by classical methods like Newton Raphson and lambda-iteration methods is difficult and inaccurate. Therefore, the application of metaheuristic methodologies to solve these types of problems is very popular. Among all evolutionary techniques, PSO [41–44] is more popular than other methods in the literature. The PSO can handle large dimension, nonconvex, nonlinear, and multiconstraint problems efficiently due to their random search technique. Despite all these advantages of PSO, with an increase in the size and complexity of the problem, PSO is sometimes stuck in local optimum solutions. PSO approach has three tunable parameters, that is, w, C_1, and C_2. Here, C_1 and C_2 are mainly random numbers. So, these parameters sometimes faced problems in handling the composite functions and struck at local optima. Therefore, a strong variant of PSO is proposed to tackle this problem. DPSO tackled all these problems because all these parameters are tuned dynamically and depend on system parameters like maximum iteration and classical PSO parameters such as velocity, position, gbest, and pbest.

The PSO method starts by selecting a population of auxiliary solutions and searching for optima via the aid of modernizing solutions. The particle's velocity has a significant impact on particular social, cognitive, and initial components. The rule for updating particle velocity demands a proper balance between the social and cognitive properties of the swarm required. Initial domination of cognitive part over social part is must to secure by exploration of search space. However, subordination of social part over cognitive is needed to propel all solutions towards global optima to enhance local exploitation. Therefore, an explored control equation is propounded for regulating particle velocity dynamically by taking constriction variables e_1 and e_2. Likewise, the cognitive and social parts are updated by considering RMS experience and preceding experience, respectively [45].

During the application of PSO, the position and velocity of each particle are updated as follows:

$$S_n^{t+1} = S_n^t + V_n^{t+1} \times \Delta t, \tag{5}$$

where Δt is the time step of 1 second.

The inertia weight is given as

$$W = W_{\min} + \frac{\left(W_{\max} - W_{\min}\right) \times \left(\mathrm{itr}_{\max} - \mathrm{itr}\right)}{\mathrm{itr}_{\max}}. \tag{6}$$

3.1. Proposed DPSO. In this study, the proposed DPSO, W, is modified by exponentially decaying function η to avoid premature convergence. $W = e^{(-\eta \ln k_w)}$, where $k_w = (w_{\min}/w_{\max})$ and $\eta = \mathrm{itr}/\mathrm{itr}_{\max}$, and the factor K_w be chosen in respect of inertia weight's bounds maximum and minimum limit. In this paper, the value of kw is the ratio of maximum and minimum bound of the inertia weight [45].

3.1.1. Proceeding Experience. Update RMS experience and acceleration coefficients and parameters of constriction factor approach where

$$\xi_1 = e^{(-\mu_1\eta)}; \xi_2 = k.e^{(\mu_2\eta)}; k = \frac{\xi_1 \cdot c_{1b}}{\xi_2 \cdot c_2}, \quad (7)$$

in which k is the proposed social and cognitive coefficients. For the identical value of these factors, $\eta = \eta_t$. All other factors valued are stated in Table 1. The flowchart for the proposed DPSO and constraint-handling management for MAED are depicted in Figures 1 and 2, respectively (Algorithm 1).

Table 1: Parameters are taken into account to deal with Test System 3.

Parameter	Value
Total power demand (MW)	10500
Tie line limit (MW)	200/100
Area load demand (%)	15/40/30/15
Population size	80
$w_{\max}$	0.9
$w_{\min}$	0.1
c_{1b}	2
c_{1p}	0.5
μ_1	5
μ_2	3.9
η_t	2/3
k	4
$itr_{\min}/itr_{\max}$	1/1000

3.2. Grey Wolf Optimizer. Grey wolf optimization (GWO) algorithm is a metaheuristic optimization recently developed by Mirjalili et al. in 2014. The algorithm is inspired by the hierarchy behaviors of grey wolves and imitates the hunting phenomena of grey wolves. Despite the various advantages of metaheuristic algorithms like those applied on nonconvex functions as system complexity increases, the GWO algorithm is free from input parameters initialization. GWO approach has two tunable parameters, a and c. So, exploration and exploitation in search space become faster. In the present algorithm, the first fittest solution is alpha (α), beta (β) is second, delta (δ) is third, and other are followers, that is, omega (ω). Wolves follow the behavior of encircling prey, pursuing, hunting, tracking, approaching, and so on [46].

3.2.1. Mathematical Modelling of GWO. In the present section, the detailed mathematical modelling of the algorithm using the social hierarchy model of wolves and group hunting of prey is presented.

3.2.2. Social Hierarchy Model. In the social hierarchy model, the fittest solution is assumed as alpha (α) wolf or the leader (first) wolf; the next solution is the beta (β) wolf or second-best solution, the delta (δ) wolf is the third-best solution among all, and the remaining solutions are omega (ω) wolves.

3.2.3. Encircling the Prey. During hunting, the grey wolves encircle the prey, and the following equations are used to model the process [46].

$$\vec{C} = \left|\vec{B} \cdot \overrightarrow{X_p(t)} - \overrightarrow{X(t)}\right|, \quad (8)$$

$$\overrightarrow{X(t+1)} = \overrightarrow{X_p(t)} - \vec{A} \cdot \vec{C}, \quad (9)$$

where t is the present iteration of the objective problem, $\overrightarrow{X_p(t)}$ represents the available position vector of the prey, $\overrightarrow{X(t)}$ represents grey wolf's position vector and the coefficient vectors $\vec{A}$, and it is calculated using the following equations.

$$\begin{aligned}\vec{A} &= 2\vec{a} \cdot \vec{r}_1 - \vec{a},\\ \vec{C} &= 2 \cdot \vec{r}_2,\end{aligned} \quad (10)$$

where $\vec{r}_1$ and $\vec{r}_2$ are random numbers between [0, 1], $a = 2 - 2\,(\text{itr}/\max \text{itr})$, where itr = present iteration and max itr = maximum number of iteration.

Here, a is decreasing linearly from 2 to 0 during each iteration. Generally, the grey wolf updates their position randomly in solution space around the prey using equations (8) and (9). This concept can be implemented for n dimensions search space.

As $\vec{A}$ is a function of $\vec{a}$ and a random vector of range [0 1]. Value of $\vec{a}$ decreases from 2 to 0 as the iteration number increases. The fluctuations range of $\vec{A}$ also decreased by $\vec{a}$. So, when the values of $\vec{A}$ are in the range of [−1 1], the new position of search agent has a position between position of prey and its current position. For $|\vec{A}| < 1$, the search agents converge toward the optimal location.

In the GWO technique, positions of search agents are updated to correspond to alpha, beta, and delta. They deviate from searching for prey and assemble to assail prey. For $|\vec{A}| > 1$, the search agents diverge from an optimal local solution to find an optimal global solution. This highlights exploration and permits the GWO algorithm to troll it globally. As the value of $\vec{a}$ decrease linearly from [2–0], so the $\vec{A}$ mainly emphasizes exploration during initial iterations. But value of $\vec{C}$ varies in [0–2] randomly, during initial as well as final iterations. So $\vec{C}$ emphasizes exploration in last iterations also for $\vec{C} > 1$.

3.2.4. Hunting. All grey wolves can capture the site and location of prey during hunting, and the positions of the wolf are updated around the prey using the following equations:

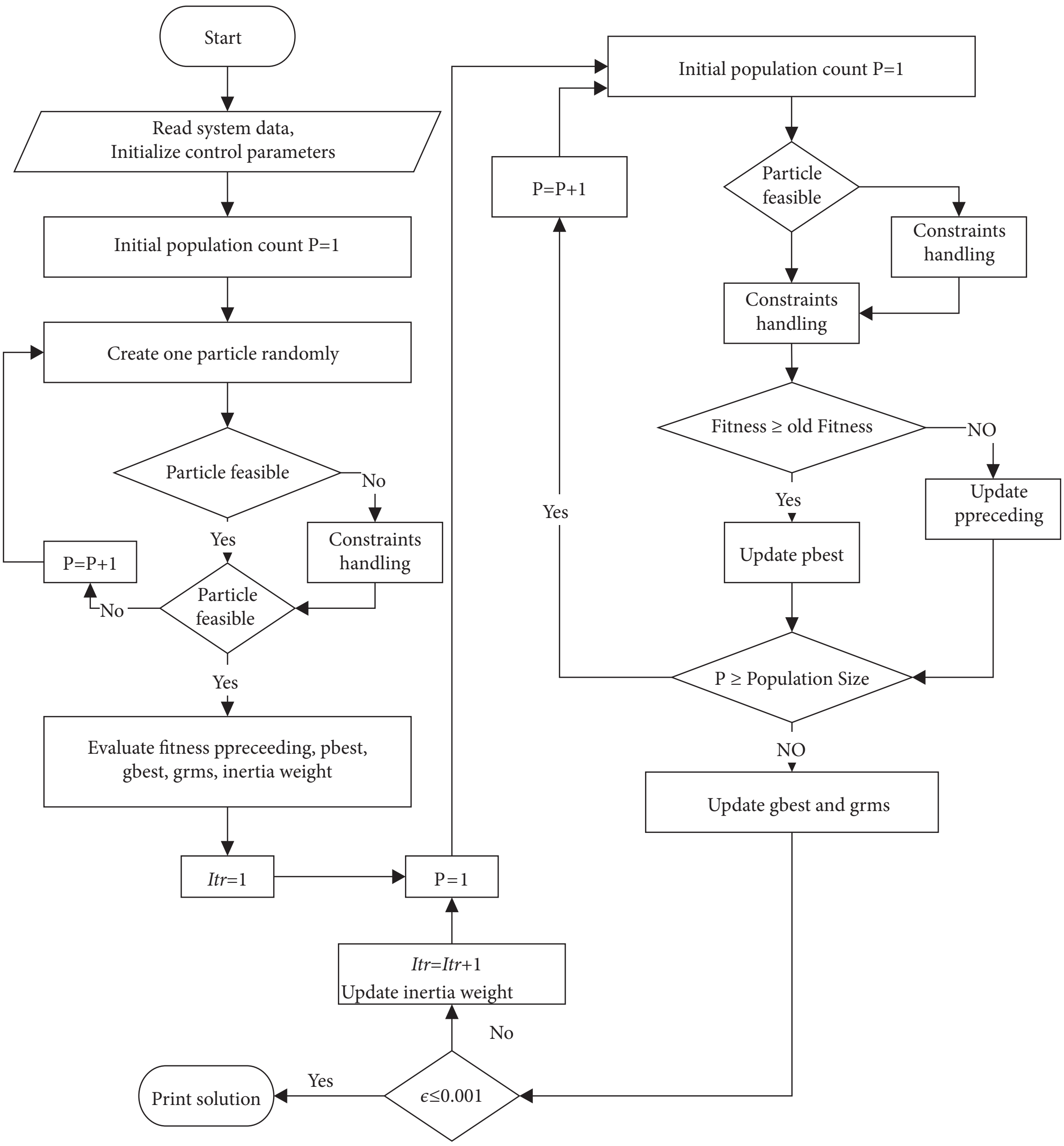

Figure 1: Flowchart for MAED using DPSO.

$$\vec{D}_\alpha = \left|\vec{C}_1 \cdot \vec{X}_\alpha(t) - \vec{X}(t)\right|,$$
$$\vec{D}_\beta = \left|\vec{C}_2 \cdot \vec{X}_\beta(t) - \vec{X}(t)\right|, \quad (11)$$
$$\vec{D}_\delta = \left|\vec{C}_3 \cdot \vec{X}_\delta(t) - \vec{X}(t)\right|,$$

$$\vec{X}_1(t) = \vec{X}_\alpha(t) - \vec{A}_1 \cdot \vec{D}_\alpha,$$
$$\vec{X}_2(t) = \vec{X}_\beta(t) - \vec{A}_2 \cdot \vec{D}_\beta, \quad (12)$$
$$\vec{X}_3(t) = \vec{X}_\delta(t) - \vec{A}_3 \cdot \vec{D}_\delta,$$

$$\vec{X}(t+1) = \frac{\left(\vec{X}_1(t) + \vec{X}_2(t) + \vec{X}_3(t)\right)}{3}, \quad (13)$$

where $\vec{X}_\alpha(t)$, $\vec{X}_\beta(t)$, and $\vec{X}_\delta(t)$ are the position of first-, second-, and third-best fitness value. $\vec{D}_a$, $\vec{D}_\beta$, and $\vec{D}_\delta$ are determined as above equations.

3.2.5. Implementation of GWO for MAED Problem. The implementation of the GWO algorithm to solve the ELD complex problem with VPL is described in Figure 3 as follows (see Algorithm 2).

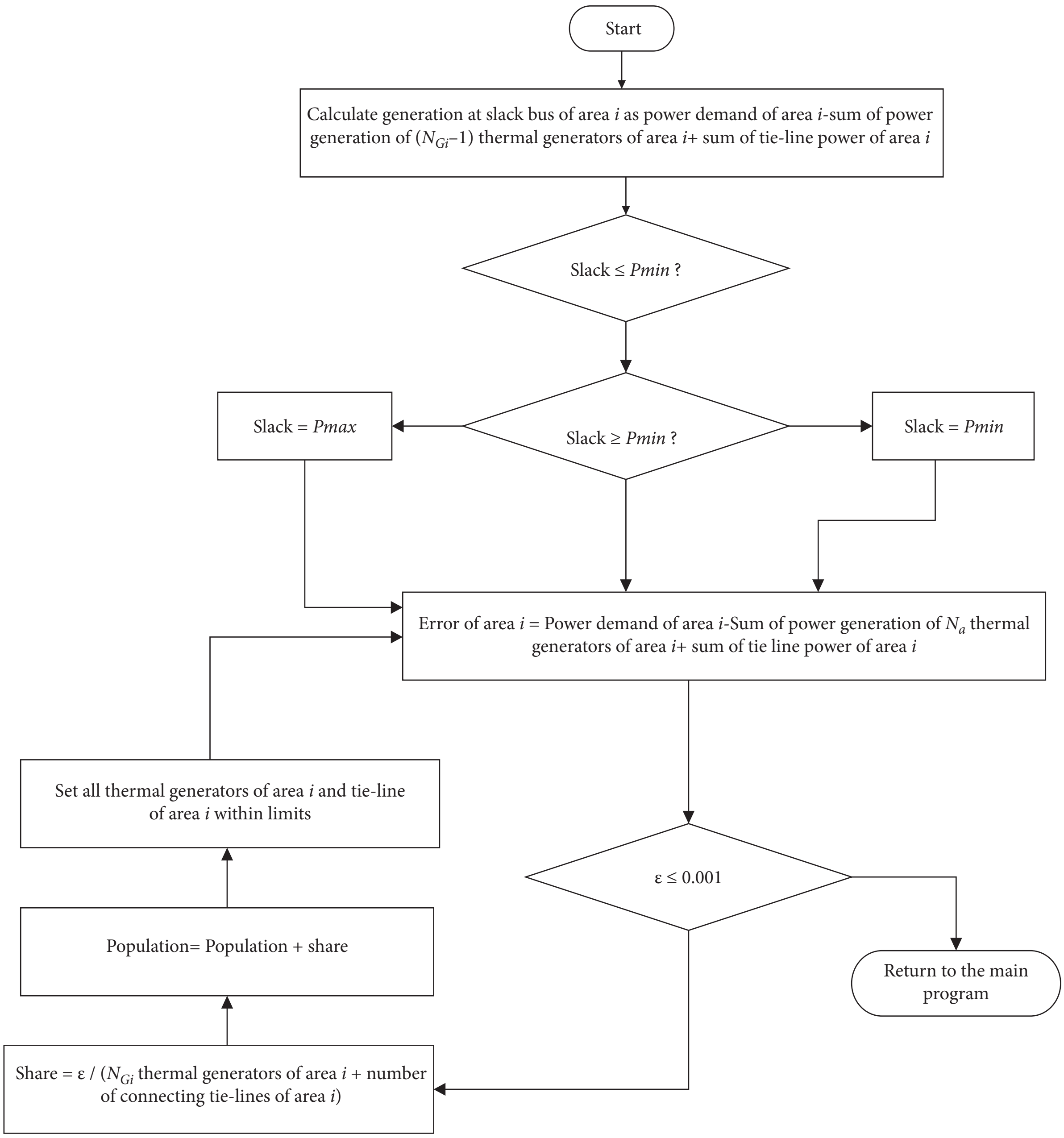

Figure 2: Constraint management algorithm of DPSO.

Step 1: enter the system data and initialize all control parameters and new particles randomly.
Step 2: check the feasibility of the current particle; if it is not feasible, then run the constraint management algorithm.
Step 3: make an increment in population count by 1. Now check the population, if it is less than its maximum value, go back to Step 1.
Step 4: calculate fitness function through (equation (1)), preceding, grms, inertia weight, and constriction function via (equations (5)–(7)).
Step 5: initialize iteration count.
Step 6: repeat Steps 1 and 2. Update preceding for the current particle. Then repeat Step 4.
Step 7: update grms and gbest.
Step 8: make an increment in iteration count by 1. If iteration did not reach its maximum value, repeat Step 8.
Step 9: print final results.

Algorithm 1: Particle encoding and initialization methodology algorithm.

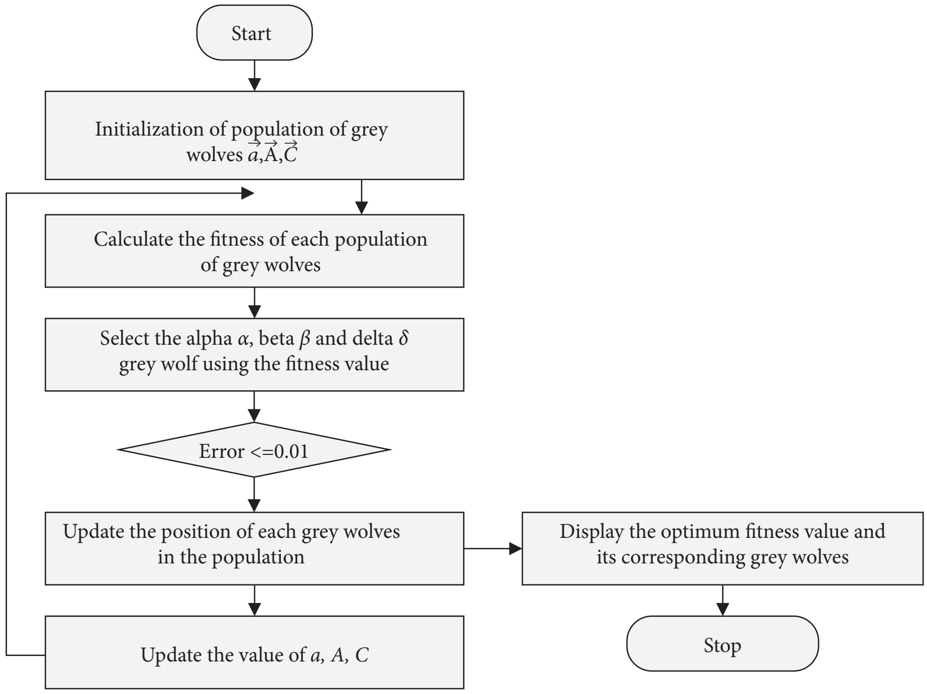

FIGURE 3: Flowchart for handling MAED problem by grey wolf optimizer.

Step 1: assign grey wolf population X_k ($k = 1, 2, \ldots, N$); N = no of generators
Step 2: initialize a, A, and C
Step 3: compute the objective function values for each search agent
Step 4: find all solutions and initializ the best solution with them
Step 5: X_α = select first leader (archive)
  X_β = select second leader (archive)
  X_δ = select third leader (archive)
  $z = 1$;
Step 6: **while** ($z < Max\ iterations$)
Step 7: **for** every variable
  Update position of present search solution by equations (8)–(13)
  end for
Step 8: modernize a, A, and C
  Compute fitness values of every solution
  Then find other solutions
    Update the solution with reference to best solutions
Step 9: **If** particle checking is full
  Run the grid mechanism to omit one of the present archive members
  Add the new solution to the archive **end if**
Step 10: **If** any new added solutions to the best solution are located shell to a hypercube
  Update the population with other new solution(s) **end if**
Step 11: X_α = select leader (archive)
  Exclude alpha from the archive temporarily to avoid selecting the same leader
  X_β = select leader (archive)
  Exclude beta from the archive temporarily to avoid selecting the same leader
    X_δ = select leader (archive)
    Add back alpha and beta to the archive
    $t = t + 1$
    end while
Step 12: return **archive**

ALGORITHM 2: Algorithm for handling MAED problem by grey wolf optimizer.

4. Results and Discussion

The constraints considered in this study made MAED problem much more complex and difficult to solve than the classical ED problem. DPSO and GWO techniques are used and tested for the MAED problem on three systems having different sizes and complexities. The performance of both DPSO and GWO variants is compared.

4.1. Description of the Test Systems

4.1.1. Test System 1: Single-Area Problem. The first type of system consists of only a single area with three generator units and no tie line connection as shown in Figure 4. Generator cost coefficients are as follows: fixed cost for 3 generators (a) is 561, 310, and 78; running cost (b) is 7.92, 7.85, and 7.97; and maintenance cost (c) is 0.001562, 0.00194, and 0.00482, respectively. This case study's upper and lower generator limit is [600, 400, and 200] and [150, 100, and 50]. The data for the test system is taken from [1].

In Table 2, results are taken by varying load demand, and results are compared from the classical method, that is, lambda-iteration method.

It is revealed from the results that all constraints are satisfied within their limits. In the above case study, power violation = zero means all constraints are satisfied and no power loss occurs. From Figure 5, it is seen that the GWO approach converges faster compared to the PSO approach.

4.1.2. Test System 2: Two-Area Problem with 1 Tie Line. The two areas with four generator units are tied through a single tie line shown in Figure 6. Generator cost coefficients adopted from literature [17, 45] are as follows: fixed cost for 4 generators (a) is 561, 310, 78, and 250; running cost (b) is 7.92, 7.85, 7.97, and 7.5; and maintenance cost (c) is 0.001562, 0.00194, 0.00482, and 0.00181 respectively. This case study's upper and lower generator limit is [600, 400, 200, and 340] and [150, 100, 50, and 70]. In this case study, the load is varied, and the corresponding tie line limit is also varied. The initial value for C_1 and C_2 is 1.8 and 0.2, respectively. The final value for C_1 and C_2 is 0.2 and 1.9, respectively. The results are concluded after 500 iterations for both methods.

From Table 3, it is seen that power mismatch is zero, and the system satisfies all the constraints within the prespecified limits.(Table 4)..

The results show the effectiveness of the GWO technique over DPSO and ABCO techniques. The generation cost and execution time are less in the case of GWO as compared to DPSO and ABCO. The DPSO saves Rs. 12.4 over ABCO approach and in the case of GWO Rs. 12.7 over ABCO.

From Figure 7, it is seen that the GWO approach converges faster compared to the PSO approach.

4.1.3. Test System 3: Four-Area System. In this system, four areas with ten generator units in each area are considered for generation, including all constraints. All the generating units included valve point loading coefficients. The areas are fully interconnected, that is, the power can flow between any two areas. Hence, the system has four areas, each consisting of 10 generators and connected with three tie lines, as shown in Figure 8. The total demand for this case is 10,500 MW. In this case study, Area 1 shares 15% load demand, Area 2 shares 40% load demand, Area 3 shares 30% load demand, and Area 4 shares 15% load demand. The tie line limit from Area 1 to Area 2, from Area 1 to Area 3, and from Area 2 to Area 3 or vice versa is taken as 200 MW and that for the remaining, each tie line is taken as 100 MW. Along with this, other data related to this case study is mentioned in Table 1. The cost coefficient data for 40 generators are adapted from [47].

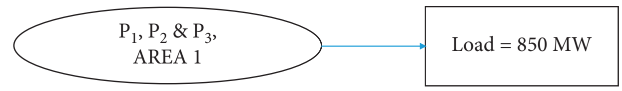

Figure 4: Test System 1: problem descriptions of 1 area and 3 generator units.

The dispatch of the current MAED problem consists of power generation of each generator for every area and the power flowing through the tie line given in the system. The dispatch schedule of the system, for the best run with minimum cost, is presented below in Table 5.

The DPSO and GWO are successfully applied to MAED in MATLAB. The scheduled dispatch of the problem specified earlier is recorded for twenty-five test runs. The total cost and CPU time taken for each dispatch have been presented in Table 6. The analysis of these runs is also done, and the results obtained are compared with other methods reported in Table 7. The Wilcoxon rank-sum test is performed on cost values of both the approaches that are obtained in 25 runs in MATLAB using the command rank-sum and that command prompt return the p value of a two-sided Wilcoxon rank-sum test equal to 2.4170×10^{-6} and h value return equal to 1 that indicates a rejection of the null hypothesis at the 5% significance level. The struct format returns zval and rank-sum values as 4.7150 and 881, respectively, for the obtained cost values.

Table 8 shows the power flow between each pair of areas. Every entry corresponds to the power flowing in the respective tie line. As can be seen below, the diagonal entries will always be zero because no tie line flows possible within the area. The MATLAB program has been run for various combinations of iteration count and population size. The cost convergence curve is a plot of fuel cost obtained versus iteration count. The curve has been plotted for iteration count and population size being one thousand and one hundred, respectively. This curve has been shown in Figure 9.

It is visible that the convergence curves obtained by solving Test System 3 using DPSO and GWO are shown in Figure 9. It is initially observed that the rate of decrease of the cost value is significant but slows down later, and GWO shows better results after complete iterations.

From Table 7, it is concluded that the GWO approach is better in terms of operating cost, execution time, and higher efficiency, keeping in mind all the constraints so that the power mismatch and violation are zero.

Table 2: Results comparison of GWO, PSO, and classical method on 25 statistical runs.

P_D (power demand) (MW)	850 (MW)			1000 (MW)		
Method	GWO	PSO	Classical method [1]	GWO	PSO	Classical method [1]
Cost (Rs/hr)	8194.4	8194.4	8194.45	9583.1	9583.2	9583.1
P1 (MW)	391.84	392.52	393.2	463.11	458.06	462.11
P2 (MW)	337.59	334.07	334.6	392.05	396.46	394.25
P3 (MW)	120.57	123.41	122.2	144.84	145.48	143.64
CPU mean time	5.89	11.85	—	7.75	12.31	---
Power violation	0.00	0.00	0.00	0.00	0.00	0.00

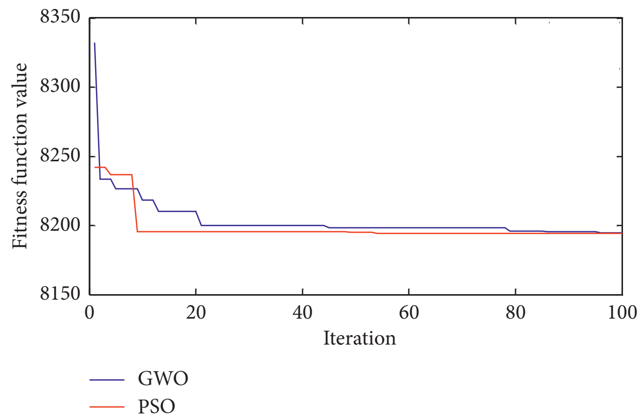

Figure 5: Convergence case of Test System 1 for both techniques.

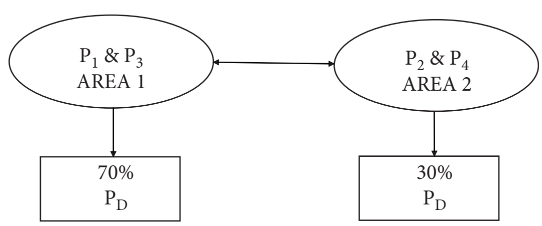

Figure 6: Test System 2: problem descriptions of 2 areas and four generator units.

Table 3: Power dispatch of 4 units according to power demand.

Power (MW)	$P_D = 1000$ (MW) (DPSO)	$P_D = 1000$ (MW) (GWO)	$P_D = 1120$ (MW) (DPSO)	$P_D = 1120$ (MW) (GWO)
P_1	381.73	381.59	444.95	422.5
P_2	195.58	194.66	215.93	211.42
P_3	118.3	118.46	139.05	167.63
P_4	304.39	305.33	320.07	318.45
Tie line power flow (MW)	199.97	199.96	200	193.87

Table 4: Cost of 4 generating units according to demand $P_D = 1120$ MW.

Method	Average cost (Rs/h)	Best cost (Rs/h)	Worst cost (Rs/h)	Mean time (CPU sec)	Standard deviation
DPSO	10,605.14439	10,605	10,605.3425	0.264437	0.063260
GWO	10,604.891	10,604.45	10,605.120	0.250588	0.056321
ABCO [24]	10,617.5431	10,608.6781	10,664.3588	4.3594	27.8354

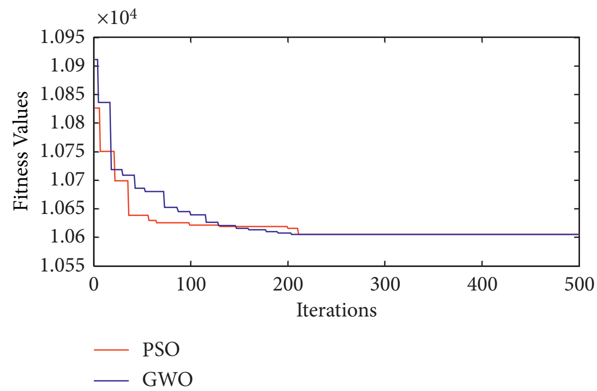

Figure 7: Convergence case of Test System 2 for both techniques.

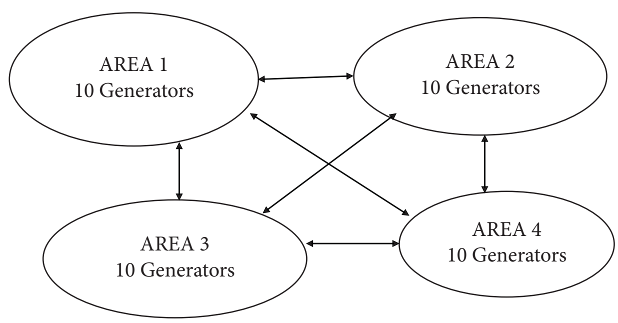

Figure 8: Problem descriptions of 4 areas, 40 generator units, and six tie lines.

Table 5: Results of power dispatch of 40 generators by both the approaches.

Generators	DCPSO (MW)	GWO (MW)	Generators	DCPSO (MW)	GWO (MW)
P_1	110.5595	114	P_{21}	523.1689	514.147
P_2	110.5595	114	P_{22}	523.1689	514.147
P_3	116.5595	66.015	P_{23}	523.1689	534.211
P_4	186.5595	83.204	P_{24}	523.1689	534.211
P_5	93.5595	97	P_{25}	523.1689	468.288
P_6	136.5595	74.3246	P_{26}	523.1689	468.288
P_7	260.2644	240.556	P_{27}	10	10
P_8	296.5595	280.241	P_{28}	10	10
P_9	296.5595	274.65	P_{29}	10	10
P_{10}	93.5595	130	P_{30}	47	97
P_{11}	94	216.98	P_{31}	190	190
P_{12}	94	205.18	P_{32}	190	190
P_{13}	125	312.94	P_{33}	190	190
P_{14}	486.610	418.54	P_{34}	168.744	200
P_{15}	486.610	422.66	P_{35}	168.744	200
P_{16}	486.610	422.66	P_{36}	168.744	200
P_{17}	486.610	500	P_{37}	110	110
P_{18}	486.610	500	P_{38}	110	110
P_{19}	536.610	550	P_{39}	110	110
P_{20}	536.610	550	P_{40}	320.744	110

Table 6: Run analysis of 25 runs of MAED using DPSO and GWO.

S. no.	Cost (Rs/h) of DPSO	Cost (Rs/h) of GWO	CPU time (s) of DPSO	CPU time (s) of GWO
1	123,738.3254	123,721.122	104.67	97.213
2	123,812.5644	123,712.325	61.53	90.534
3	123,877.6792	123,723.631	137.05	109.054
4	123,882.7808	123,792.833	115.45	94.658
5	123,759.8648	123,612.173	65.20	91.983
6	123,818.2971	123,623.243	59.45	87.449
7	123,738.3254	123,125.108	148.94	91.023
8	123,843.1507	123,612.793	147.37	88.998
9	123,776.3162	123,625.108	148.21	86.480
10	123,777.5035	123,593.503	155.19	87.001
11	123,847.6935	123,693.034	147.91	86.802
12	123,798.0078	123,572.307	61.02	89.112
13	123,717.4591	123,661.283	138.72	87.124
14	123,657.4212	123,724.197	140.33	87.501
15	123,599.2091	123,622.873	140.62	92.043
16	123,823.4058	123,599.024	133.54	87.009
17	123,764.0492	123,625.263	129.55	90.641
18	123,830.4886	123,656.898	106.70	87.608
19	123,881.4434	123,597.098	94.81	90.700
20	123,881.6	123,770.425	122.99	94.321
21	123,705.8138	123,711.371	76.46	93.112
22	123,722.2477	123,707.126	93.86	93.001
23	123,800.1607	123,605.183	108.31	86.992
24	123,935.3665	123,787.937	98.42	92.861
25	123,782.9852	123,591.523	119.06	90.992
Average	123,790.8864	123,642.695	114.21	90.986
Minimum	123,599.2091	123,572.307	59.45	86.48
Maximum	123,935.3665	123,792.833	148.94	109.05
Standard deviation	77.1306	66.65618	31.0525	4.779

Table 7: Result comparison of the identical problem by various techniques earlier and by both techniques.

Method	Best cost	Avg. cost	Worst cost	Mean CPU time (s)
ABCO [24]	1,24,009.4	—	—	126.9
DE [24]	—	1,24,544.1	—	134.8
EP [24]	—	1,24,574.5	—	144.5
HCPSOGA [31]	1,23,531.2	—	—	190.58
RCGA [28]	1,28,046.50	—	—	—
PSO [35]	1,28,403	—	—	—
IGOA [35]	1,23,273	—	—	—
FPA [34]	1,23,999.2	—	—	—
DPSO	1,23,599.20	1,23,790.88	1,23,935.36	114.2
GWO	1,23,125.108	1,23,642.695	1,23,792.833	90.986

Note: "—": values are not given in papers.

Table 8: Tie line results of Test System 3.

Tie line limit (MW)	By DCPSO (MW)	By GWO (MW)
1–2	107.5098	198.12
1–3	47.4277	−1.0910
1–4	7.8029	−99.9093
2–3	−186.610	−1.09910
2–4	−86.61	−99.9093
3–4	−73.1689	8.1111

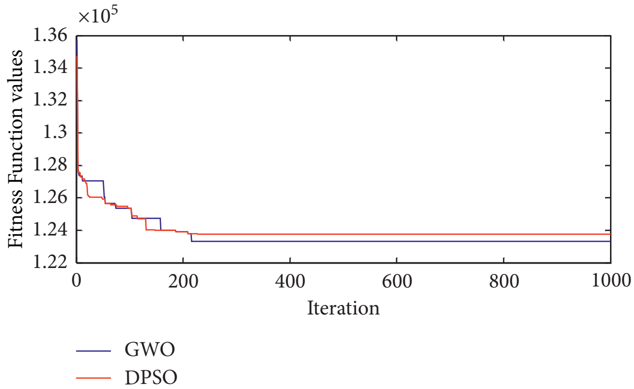

Figure 9: Convergence case of Test System 3 for both techniques.

5. Conclusion

In this paper, the DPSO and GWO have been applied successfully to model and solve the multiarea economic dispatch in three different test cases. First, the MAED problem with nonlinear cost function is solved on a single-area test system consisting of 3 thermal generators. Second, DPSO and GWO are applied on two-area test systems with four thermal units with single tie lines. These are, after that, employed on a multiarea test system consisting of 40 thermal units and six tie lines. Optimum demand sharing of power generating units is evaluated using DPSO and GWO optimization techniques. The simulation results reveal that GWO techniques produce qualitative cost solutions without any constraint violation. A significant improvement in the cost results has been obtained compared to other optimization techniques discussed in the literature. In the future, this work can be extended to work in deregulated, stochastic, and contingent environments. The losses can also be calculated using the B-coefficients of thermal generators in future research work. Ramp rate is also an important constraint that makes power system problems more realistic and can also be considered in future research work.

Nomenclatures

a_{ij}, b_{ij}, and c_{ij}: The cost coefficients of the jth generator in area i (Rs/hr), (Rs/hr MW^{-1}), and (Rs/hr MW^{-2})

C_1 and C_2: Acceleration coefficients for the best and social experience of PSO

C_{1b} and C_{1p}: Acceleration coefficients for best and preceding experience

e_{ij} and f_{ij}: The valve point effect coefficients of the jth generator in area i (Rs/hr, MW^{-1})

$g\text{best}^t$: The best particle during tth iteration

$g\text{rms}^t$: Root mean the square experience of the swarm during tth iteration

itr: Current iteration count

$\text{itr}_{\max}$: Maximum iteration count

P_{Gij}: The real power output of the jth generator in area i (MW)

$P_{G_{ij}}^{\min}/P_{G_{ij}}^{\max}$: Minimum/maximum generation limits of jth generator in area i (MW)

$P_{Tim}^{\min}/P_{Tim}^{\max}$: Minimum/maximum tie line power limit from area i to area m (MW)

preceding_n: Preceding position of nth particle achieved based on its just previous experience

P_{Tim}: Tie line real power flow from area i to area m (MW) $\text{rand}_1()$ and $\text{rand}_2()$ random numbers in [0, 1]

V_n^t:The velocity of nth particle at tth iteration$W$: The velocity of nth particle at tth iteration$W$:Inertia weight

PSO: Particle swarm optimization

GWO: Grey wolf optimizer

RCGA: Real codec genetic algorithm

ABCO: Artificial bee colony optimization

MAED: Multiarea economic dispatch

P_{Gi}: Total real power generation in area i (MW)

k:The ratio of dynamic cognitive and social acceleration coefficients: The ratio of dynamic cognitive and social acceleration coefficientsk_w: The ratio of maximum and minimum bound of the inertia weight

M: Number of areas

N_{Gi}: Number of generating units in the system in area i

P_{Di}: The total real power demand of area i (MW)

$P\text{best}_n$: The best position of nth particle achieved based on its own experience

PD: The total actual power demand of the system (MW)

$W_{\min}/W_{\max}$: Minimum/maximum value of inertia weight

Δt: Time step (s)

ζ_1 and ζ_2: Exponential constriction functions

η: The ratio of the current and maximum iteration count

$η_t$: The value of g at which cognitive and social behavior equalizes

μ: Constant

μ_1 and μ_2: Coefficients of exponent terms

PSO-TVAC: PSO time-varying acceleration coefficients

DE: Differential evolution
EP: Evolutionary programming
DPSO: Dynamically controlled particle swarm optimization
ED: Economic dispatch.

Data Availability

The data used in this study are available from the corresponding author upon request.

Conflicts of Interest

The authors declare that they have no conflicts of interest.

References

[1] A. J. Wood and B. F. Wollenberg, *Power Generation Operation and Control*, Wiley Publication, New York, NY, USA, 2013.

[2] K. P. Wong and C. C. Fung, "Simulated annealing based economic dispatch algorithm," *IEEE Proceedings C Generation, Transmission and Distribution*, vol. 140, no. 6, pp. 509–515, 1993.

[3] D. C. Walters and G. B. Sheble, "Genetic algorithm solution of economic dispatch with valve point loading," *IEEE Transactions on Power Systems*, vol. 8, no. 3, pp. 1325–1332, 1993.

[4] H. T. Yang, P. C. Yang, and C. L. Huang, "Evolutionary programming based economic dispatch for units with non-smooth fuel cost functions," *IEEE Transactions on Power Systems*, vol. 11, no. 1, pp. 112–118, 1996.

[5] C. T. Lin and C. T. Lin, "New approach with a Hopfield modeling framework to economic dispatch," *IEEE Transactions on Power Systems*, vol. 15, no. 2, pp. 541–545, 2000.

[6] Y. H. Hou, Y. W. Wu, L. J. Lu, and X. Y. Xiong, "Generalized ant colony optimization for economic dispatch of power systems," *Int. Conf. Power System Technology*, vol. 1, pp. 225–229, 2002.

[7] Z.-L. Gaing, "Particle Swarm Optimization to solving the economic dispatch considering the generator constraints," *IEEE Transactions on Power Systems*, vol. 18, no. 3, pp. 1187–1195, 2003.

[8] B. K. Panigrahi, S. R. Yadav, S. Agrawal, and M. K. Tiwari, "A clonal algorithm to solve economic load dispatch," *Electric Power Systems Research*, vol. 77, no. 10, pp. 1381–1389, 2007.

[9] S.-K. Wang, J.-P. Chiou, and C.-W. Liu, "Non-smooth/non-convex economic dispatch by a novel hybrid differential evolution algorithm," *IET Generation, Transmission & Distribution*, vol. 1, no. 5, pp. 793–803, 2007.

[10] B. K. Panigrahi and V. Ravikumar Pandi, "Bacterial foraging optimisation: Nelder-Mead hybrid algorithm for economic load dispatch," *IET Generation, Transmission & Distribution*, vol. 2, no. 4, pp. 556–565, 2008.

[11] A. Bhattacharya and P. K. Chattopadhyay, "Biogeography-based optimization for different economic load dispatch problems," *IEEE Transactions on Power Systems*, vol. 25, no. 2, pp. 1064–1077, 2010.

[12] R. Shoults, S. Chang, S. Helmick, and W. Grady, "A practical approach to unit commitment, economic dispatch and savings allocation for multiple-area pool operation with import/export constraints," *IEEE Transactions on Power Apparatus and Systems*, vol. 99, no. 2, pp. 625–635, 1980.

[13] T. Yalcinoz and M. J. Short, "Neural networks approach for solving economic dispatch problem with transmission capacity constraints," *IEEE Transactions on Power Systems*, vol. 13, no. 2, pp. 307–313, 1998.

[14] D. Streiffert, "Multi-area economic dispatch with tie line constraints," *IEEE Transactions on Power Systems*, vol. 10, no. 4, pp. 1946–1951, 1995.

[15] C. L. Nanming Chen and N. Chen, "Direct search method for solving economic dispatch problem considering transmission capacity constraints," *IEEE Transactions on Power Systems*, vol. 16, no. 4, pp. 764–769, 2001.

[16] P. S. Manoharan, P. S. Kannan, S. Baskar, and M. Willjuice Iruthayarajan, "Evolutionary algorithm solution and KKT based optimality verification to multi-area economic dispatch," *International Journal of Electrical Power & Energy Systems*, vol. 31, no. 7-8, pp. 365–373, 2009.

[17] M. Sharma, M. Pandit, and L. Srivastava, "Reserve constrained multi-area economic dispatch employing differential evolution with time-varying mutation," *International Journal of Electrical Power & Energy Systems*, vol. 33, no. 3, pp. 753–766, 2011.

[18] G. R. Venkatakrishnan, J. Mahadevan, and R. Rengaraj, "Grey Wolf Optimizer for economic load dispatch with valve point loading," *International Journal of Advances in Engineering & Technology*, vol. 7, pp. 158–163, 2016.

[19] A. V. V Sudhakar, K. Chandaran, and A. Jaya Laxmi, "Differential evolution for solving multi-area economic dispatch," in *Proceedings of the 2014 International Conference on Advances in Computing, Communications and Informatics (ICACCI)*, Delhi, India, September 2014.

[20] M. Yoshimi, K. S. Swarup, and Y. Izui, "Optimal economic power dispatch using genetic algorithms," in *Proceedings of the Second International Forum on Applications of Neural Networks to Power Systems [1993]*, pp. 157–162, Yokohama, Japan, April 1992.

[21] K. Y. Lee and M. A. El-Sharkawi, *Modern Heuristic Search Techniques*, Wiley Publication, Hoboken, NJ, USA, 2008.

[22] V. K. Kamboj, S. K. Bath, and J. S. Dhillon, "Solution of non-convex economic load dispatch problem using grey wolf optimizer," *Neural Computing & Applications*, vol. 25, no. 7, 2015.

[23] K. Jain and M. Pandit, "Discussion of "Reserve constrained multi-area economic dispatch employing differential evolution with time-varying mutation" by Manisha Sharma et al. "International Journal of Electrical Power and Energy Systems," 33 March (2011) 753-766," *International Journal of Electrical Power & Energy Systems*, vol. 39, no. 1, pp. 68-69, July 2012.

[24] N. H. Marzuki, N. A. Rahmat, J. Mat Salleh, and O. F. Otoh, "Multi-area economic dispatch by UsingDifferential evolution immunized ant ColonyOptimization (DEIANT)," *International Journal of Engineering and Advanced Technology*, vol. 1, no. 1, pp. 3525–3530, 2019.

[25] K. Advik and V. Kaur, "A novel optimization plan for multiple-area economic dispatch: an electro search optimization approach," *Munich Personal RePEc Archive*, pp. 1–12, 2018, https://mpra.ub.uni-muenchen.de/88979/.

[26] M. Yazdandoost, P. Khazaei, S. Saadatian, and R. Kamali, "Distributed optimization strategy for multi area economic dispatch based on electrosearch optimization algorithm," in *Proceedings of the IEEE WAC Conference*, pp. 1–6, Stevenson, WA, USA, June 2018.

[27] M. J. Mokarram, M. Gitizadeh, T. Niknam, and S. Niknam, "Robust and effective parallel process to coordinate multi-area economic dispatch (MAED) problems in the presence of

uncertainity," *IET Generation, Transmission & Distribution*, vol. 13, no. 18, pp. 4197–4205, 2019.

[28] L. Lakshminarasimman, M. Siva, and R. Balamurugan, "Water Wave optimization algorithm for SolvingMulti-area economic dispatch problem," *International Journal of Computer Application*, vol. 167, no. 5, pp. 1–9, 2017.

[29] S. Vijayaraj, P. Dayanithi, P. P. Arjun, N. Varaprasad, K. Parthasarathy, and R. Chandrasekaran, "Multi-area economic dispatch with multi-fuel option using krill Herd algorithm," *Turkish Journal of Computer and Mathematics Education*, vol. 12, no. 12, pp. 1017–1026, 2021.

[30] B. Mandala and P. K. Roy, "Dynamic economic dispatch problem in hybrid wind based power systems using oppositional based chaotic grasshopper optimization algorithm," *Journal of Renewable and Sustainable Energy*, vol. 13, no. 1, 2021.

[31] E. Ehab and Elattar, "Solving multi-area economic dispatch with multiple fuels using hybrid optimization technique," *Mansoura Engineering Journal (MEJ)*, vol. 40, no. 3, pp. 1–12, 2015.

[32] V. P. Sakthivel and P. D. Sathyab, "Squirrel search optimization for non-convex multi-area economic dispatch," *IJE Transactions A: Basics*, vol. 34, no. 1, pp. 120–127, 2021.

[33] J. Kishore Pattanaik, M. Basu, and D. Prasad Dash, "Review on application and comparison of metaheuristic techniques to multi-area economic dispatch problem," *Prot Control Mod Power Syst*, vol. 2, no. 17, 2017.

[34] V. Chaudharya, H. M. Dubey, M. Pandita, and J. ChandBansal, "Multi-area economic dispatch with stochastic wind power using salp swarm algorithm," *Array*, vol. 8, 2020.

[35] P. Zhang, W. Ma, Y. Dong, and B. D. Rouyendegh, "Multi-area economic dispatching using improved grasshopper optimization algorithm," *Evolving Systems*, pp. 1–11, 2019.

[36] V. P. Sakthivel, M. Murugesan Suman, and P. D. Sathya, "Robust multi-area economic dispatch using Coulomb's and Franklin's laws based optimizer," *International Journal of Engineering and Technology Innovation*, vol. 10, no. 4, pp. 235–251, 2020.

[37] M. Basu, "Fast convergence evolutionary programming for multi-area economic dispatch," *Electric Power Components and Systems*, vol. 45, no. 15, pp. 1–9, 2017.

[38] M. Basu, "Artificial bee colony optimization for multi-area economic dispatch," *International Journal of Electrical Power & Energy Systems*, vol. 49, pp. 181–187, 2013.

[39] M. Pandit, K. Jain, H. M. Dubey, and R. Singh, "Large scale multi-area static/dynamic economic dispatch using nature inspired optimization," *Journal of The Institution of Engineers (India): Series B*, vol. 98, no. 2, pp. 221–229, 2016.

[40] H. Narimani, S.-E. Razavi, A. Azizivahed et al., "A multi-objective framework for multi-area economic emission dispatch," *Energy*, vol. 154, pp. 126–142, 2018.

[41] R. Eberhart, Y. Shi, and J. Kennedy, *Swarm Intelligence*, Elsevier, Amsterdam, Netherlands, 2001.

[42] P. J. Angeline, "Evolutionary optimization versus particle swarm optimization: philosophy and performance differences," *Lecture Notes in Computer Science*, Springer, vol. 1447, pp. 601–610, , Berlin, Germany, 1998.

[43] M. Clerc and J. Kennedy, "The particle swarm—explosion, stability, and convergence in a multidimensional complex space," *IEEE Transactions on Evolutionary Computation*, vol. 6, no. 1, pp. 58–73, 2002.

[44] F. Wang and Y. Qiu, "A modified particle swarm optimizer with roulette selection operator," in *Proceedings of the IEEE Proceeding of NLP-KE'05*, pp. 765–768, Wuhan, China, October-November 2005.

[45] V. K. Jadoun, N. Gupta, K. R. Niazi, and A. Swarnkar, "Multi-area economic dispatch with reserve sharing using dynamically controlled particle swarm optimization," *International Journal of Electrical Power & Energy Systems*, vol. 73, pp. 743–756, 2015.

[46] S. Mirjalili, S. M. Mirjalili, and A. Lewis, "Grey wolf optimizer," *Advances in Engineering Software*, vol. 69, p. 4661, 2014.

[47] http://www.alroomi.org/multimedia/Economic_load_dispatch/4Units/40Units_ELD test-System.

Hindawi
Mathematical Problems in Engineering
Volume 2021, Article ID 4913824, 12 pages
https://doi.org/10.1155/2021/4913824

Research Article

Regression-Based Prediction of Power Generation at Samanalawewa Hydropower Plant in Sri Lanka Using Machine Learning

Piyal Ekanayake,[1] **Lasini Wickramasinghe**,[1] **J. M. Jeevani W. Jayasinghe**,[1] **and Upaka Rathnayake**[2]

[1]*Faculty of Applied Sciences, Wayamba University of Sri Lanka, Kuliyapitiya, Sri Lanka*
[2]*Department of Civil Engineering, Faculty of Engineering, Sri Lanka Institute of Information Technology, Malabe, Sri Lanka*

Correspondence should be addressed to J. M. Jeevani W. Jayasinghe; jeevani@wyb.ac.lk

Received 9 May 2021; Revised 19 June 2021; Accepted 26 July 2021; Published 31 July 2021

Academic Editor: Tzung-Pei Hong

This paper presents the development of models for the prediction of power generation at the Samanalawewa hydropower plant, which is one of the major power stations in Sri Lanka. Four regression-based machine learning and statistical techniques were applied to develop the prediction models. Rainfall data at six locations in the catchment area of the Samanalawewa reservoir from 1993 to 2019 were used as the main input variables. The minimum and maximum temperature and evaporation at the reservoir site were also incorporated. The collinearities between the variables were investigated in terms of Pearson's and Spearman's correlation coefficients. It was found that rainfall at one location is less impactful on power generation, while that at other locations are highly correlated with each other. Prediction models based on monthly and quarterly data were developed, and their performance was evaluated in terms of the correlation coefficient (R), mean absolute percentage error (MAPE), ratio of the root mean square error (RMSE) to the standard deviation of measured data (RSR), BIAS, and the Nash number. Of the Gaussian process regression (GPR), support vector regression (SVR), multiple linear regression (MLR), and power regression (PR), the machine learning techniques (GPR and SVR) produced the comparably accurate prediction models. Being the most accurate prediction model, the GPR produced the best correlation coefficient closer to 1 with a very less error. This model could be used in predicting the hydropower generation at the Samanalawewa power station using the rainfall forecast.

1. Introduction

Hydropower is one of the most widely used green energy sources in the world today. It is not only renewable but also highly reliable in generating and supplying power to national grids. Usually, major hydropower plants are used to generate electricity for the peak requirement of the countries. Most importantly, hydropower can be generated at a relatively low cost compared to other sources like thermal power. Therefore, there is an extensive demand for hydropower development in today's world. For example, Norway produces more than 95% of its energy requirement by hydropower while many other countries such as China, United States, Brazil, and Canada also produce more and more hydropower to meet their energy demands. This is mainly to achieve sustainable energy generation goals defined by the countries themselves.

Hydropower in Sri Lanka also plays an important role as the country now depends largely on thermal power generated by using imported coal and fuel oil. Sri Lanka was successful in generating green energy in the 1990s, but not much progress could be made due to the sudden increase in demand. Recent statistics indicate that Sri Lanka has produced an average of one-fifth of its energy demand from hydropower sources. Even though Sri Lanka has planned to enhance the generation of renewable power, there is little room for the construction of new major hydropower plants beyond the existing network of power stations. Out of the four types of hydropower development, viz., run-of-river, storage, pumped storage, and offshore hydropower plants, the first two types are very common in Sri Lanka, but the other types are still under discussion. Among the hydropower plants of storage type, the Samanalawewa hydropower development scheme showcases some important features due to its location (located in Sabaragamuwa province) and the relative high capacity for power generation. This hydropower plant is in the water rich Walawe basin, and the reservoir draws much attention not only from the perspective of the hydropower development but also due to its capacity as a primary source for irrigational purposes. Moreover, the hydropower scheme at Samanalawewa has drawn much attention due to a seepage leak from the reservoir. In this context, identifying the impact of climate change on the water resources is highly important for the Samanalawewa hydropower plant. Though a couple of studies addressed this problem recently, a comprehensive research on the prediction of power generation based on all related weather indices has not yet been conducted [1].

In a nonparametric statistical analysis of the monthly data over 26 years of the catchment rainfall associated with the Samanalawewa power plant in Sri Lanka, Dabare et al. [1] showed a positive correlation between the rainfall and the hydropower generation. While proposing nonlinear analysis for more specific conclusions, this study disavowed concerns on the negative impact of climate change on the rainfall. However, Suleiman and Ifabiyi [2] have revealed that the reservoir variables of inflow, storage, and the turbine release are strongly and positively correlated with the rainfall by analyzing the rainfall data around the Shiroro hydropower dam in Nigeria since 1990. Furthermore, they reported that the optimized turbine releases ensured the year-round power generation by the reservoir storage. However, a study on the impact of rainfall and temperature on electricity generation in Ghana pointed out that instability in climate dependent hydrology could cause uncertainties in hydropower generation [3].

Artificial neural network (ANN) was widely used to develop hydropower prediction models. Khaniya et al. [4] applied seven training algorithms in the ANN technique to predict the future power generation from 2020 to 2050 at the Samanalawewa hydropower plant in Sri Lanka using rainfall data for training and validation. Of these seven algorithms, the Quasi Newton algorithm outperformed the others in forecasting the hydropower to be generated within the next three decades for two climatic scenarios. This research further pointed out that other reservoir variables such as air temperature and humidity could also be used at the input layer of the model along with the other variables, such as reservoir inflow storage, turbine release, etc., which affect energy generation. A futuristic study was carried out to assess the impact of climate change on hydropower generation in Iran for two 3-decade periods (2020–2049 and 2070–2099) based on two climatic scenarios predicted by a regional climate model, in which the rainfall and hydropower generation were simulated by an ANN and a reservoir model [5]. This study found a positive impact of climate change on hydropower generation whose greater increase occurred during the first 3-decade period than the second. However, Beheshti et al. [5] expressed reservations on the uncertainties in predicting reservoir variables and hydropower under climate scenarios and suggested further studies, taking the variability in water allocation for irrigation into account. In addition, the complex nonlinear relationship between the rainfall and minihydropower generation in gauged and ungauged catchments of Sri Lanka has been studied recently using ANN, which showed a good correlation between them at the gauged catchments compared to ungauged catchments [6]. Based on the correlation values between the observed and predicted energies, Abdulkadir et al. [7] justified the use of neural network approaches in modelling the hydropower generation as a function of reservoir variables at two reservoirs along the River Niger in Nigeria. Developing predictive models of the hydropower generation in the Amazon, Lopes et al. [8] presented a comparative analysis between polynomial and ANNs using rainfall as the only input. Using three algorithms, group method of data handling (GMDH), ANN with Levenberg–Marquardt (ANN-LM), and ANN with Bayesian regulation (ANN-BR), it was shown that GMDH is the most appropriate algorithm to optimize the model result because of its adroitness in selecting the variables at the model entry layer and that ANN-LM algorithm failed to live up to expectations due to largely dispersed data and less accuracy.

Boadi and Owusu [9] used regression analysis to quantify the fluctuations in hydropower generation at the Akosombo hydroelectric power station in Ghana and emphasized the urgency in exploring alternative power sources to overcome energy security issues for sustainable development. Having used data over two consecutive 2-decade periods (1970–1990 and 1991–2010), their study reported that 21% of interannual fluctuation in power generation is accounted for by the rainfall variability, and that 72.4% of the same is explained by the El Niño-southern oscillation (ENSO) phenomenon and the lake water level. In another study, the streamflow and the potential hydropower generation were modelled using a data-based methodology in Mid Wales, where the projected impact of climate change on a hypothetical small power plant was assessed [10]. Its results showed an increase (decrease) in the streamflow and power output during winter (summer) months. Furthermore, Khaniya et al. [11] applied the Mann–Kendall test and Sen's slope estimator tests in a trend analysis to assess the performance of a minihydropower station in Sri Lanka based on 30-years of rainfall data and 6 years of electricity generation associated with the power plant. This study proved a positive rainfall trend at several rain gauging stations except in November and January while assuring the stability of the catchment area in the wake of climate variability. Nevertheless, research on regression-based prediction models to predict the hydropower generation in Sri Lanka is highly limited. Therefore, this research focuses on developing regression-based prediction models to predict the hydropower development capacity of the Samanalawewa hydropower development scheme.

In the next section on study area and data, the Samanalawewa catchment area, meteorological data used, and their relationship to power generation are elaborated.

Section 3 describes the regression techniques, methodology, and the evaluation criteria of the model performance. Section 4 presents the results and discussion where the models developed on monthly data, models based on quarterly rainfall data, and the salient features of the meteorological factors used are explained along with a comparison on findings from similar research work in some other countries. The paper is wrapped up with the major conclusions in Section 5.

2. Study Area and Data

2.1. Samanalawewa Catchment Area. Samanalawewa hydropower plant and its reservoir are in the Balangoda area in the Ratnapura district of Sri Lanka (coordinates of the power plant are 06°40′48″N, 80°47′54″E). The construction of the dam commenced in 1986 and commissioned in 1992. The project was carried out with financial support from Japan and the United Kingdom. It is a major hydropower scheme in the country and based on the Walawe River. The dam has a height of 110 m from its foundation and is 530 m in length. It is a rock-filled dam and holds 218 million m^3 of water out of 278 million m^3 of total capacity. The balance 60 million m^3 is kept for the dead storage [12].

The catchment area of the Samanalawewa reservoir is presented in Figure 1. The catchment area is around 372 km^2 and lies in the wet zone of the country, which receives a significant annual rainfall (annual average of 2867 mm) [13]. Therefore, the reservoir has a good overall water capacity throughout the year and generates 124 MW of electricity using two turbines.

A seepage leak was identified in the reservoir while it was under construction. Though it was treated at that time, the leakage continued even after the construction. As this is not through the dam, it has not caused any instability to the dam. The seepage is measured to be 2 m^3/s and, thereafter, that lost water is used to run a minihydropower station. For this reason, the Samanalawewa reservoir and the dam have captured the interest of power engineers. Due to all these reasons, it is highly important to analyze the hydropower scheme in light of changing climate and to forecast the power generation using key reservoir variables.

2.2. Meteorological Data and Their Observational Relationships to Power Generation

2.2.1. Rainfall Data. Twenty-six (26) years of rainfall data from 1993 to 2019 measured at 6 locations in the catchment area, Alupola, Detanagalla, Balangoda, Nagarak Estate, Belihuloya, and Nanperial, were purchased from the Department of Meteorology, the state repository of climate data in Sri Lanka. The highest mean annual rainfall during this period (4272 mm) was recorded at Alupola and the lowest (2170 mm) at Balangoda, while the other locations of Detanagalla, Nagarak Estate, Belihuloya, and Nanperial had received 2843 mm, 2247 mm, 2785 mm, and 2330 mm of annual mean rainfall, respectively. Table 1 shows the summary of major statistics (minimum, maximum, average, and standard deviation) of the monthly rainfall data at the six locations.

Coherent with the above mean annual figures, the highest and the lowest monthly average rainfalls (358 mm and 183 mm) are also reported from Alupola and Balangoda, respectively. The minimum values indicate that three locations (Nagarak Estate, Belihuloya, and Nanperial) have received no rainfall (0 mm) during the months mentioned in Table 1, while Detanagalla has experienced the highest monthly rainfall (1371 mm) in November 2006.

Figure 2 shows the monthly rainfall averaged over the period, 1993–2019, at the six locations in the catchment area. It can be seen that heavy rainfall has prevailed at each location during the months of April and November, which fall within the South-west and North-east monsoon periods of the country, respectively, and the slightly higher values in November imply the greater effect of the North-east monsoon than the South-west monsoon on the rainfall in the catchment area. It is also obvious that except at one location (Alupola), the least rainfall (upto 100 mm) has occurred during the 4-month period from June to September, which is less than one-third of the heavy rainfall during the monsoon periods.

Except during the 3 months from December to February, the solitary location of Alupola has continued to receive much higher rainfall producing the highest mean annual and the highest monthly average noticed in Table 1.

2.2.2. Evaporation Data. Figure 3 shows the monthly mean evaporation at the Samanalawewa reservoir site during the period from 1993 to 2019. According to this figure, the highest monthly mean evaporation (>4.5 mm) occurs during the 4-month period from June to September, which coincides with the same period with the least monthly rainfall averaged over the period of data at five locations described in Figure 2. The period from November to January indicates the lowest mean evaporation (<3.45 mm), while the monthly mean evaporation from February to October is greater than 4 mm. It can also be traced that subdued mean evaporation in April and November correspond to the monthly rainfall averages peaked in the same months, as shown in Figure 3.

2.2.3. Temperature Data. Figure 4 depicts the monthly mean maximum and minimum temperatures with their maxima and minima at the reservoir site for the period of 1993–2019. The lowest maximum temperature prevails during the cooler months of November to January, which picks up in February and maximizes in March and April. After the cooler months, the maximum temperature hovers between 33.8°C and 34.0°C and remains approximately the same (34–34.2°C) through the warmer months of July to September. Similarly, the minimum temperature reaches its lowest figures during the same cooler months but attains the highest values within 23.8°C to 24.4°C during June to August period. It picks up steadily from January to June and decreases gradually towards the cooler months.

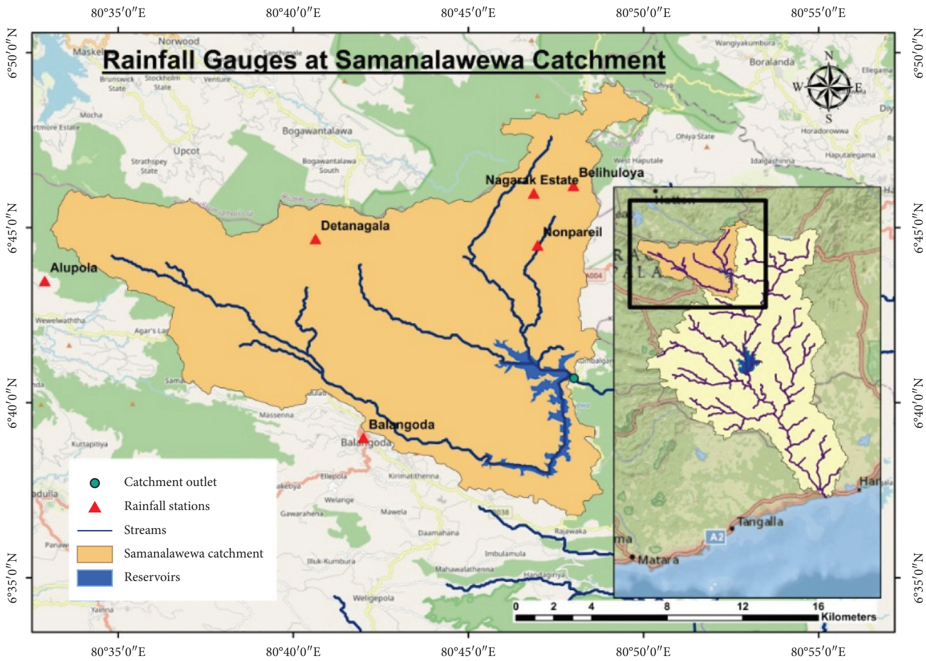

Figure 1: Catchment area of Samanalawewa reservoir.

Table 1: Summary of monthly rainfall data.

Location	Alupola (RF_1)	Detanagalla (RF_2)	Balangoda (RF_3)	Nagarak Estate (RF_4)	Belihuloya (RF_5)	Nanperial (RF_6)
Minimum rainfall (mm) and month occurred	24.5 12/1996	2.7 09/2016	4.7 05/1996	0.0 01/2009 02/2009 06/2012	0.0 09/2016	0.0 08/2001 07/2002
Maximum rainfall (mm) and month occurred	1160 05/2016	1371 11/2006	735 04/2015	661 11/2012	926 11/2012	930 11/2006
Average rainfall (mm)	358	239	183	188	233	193
Standard deviation (mm)	202	189	146	153	211	181

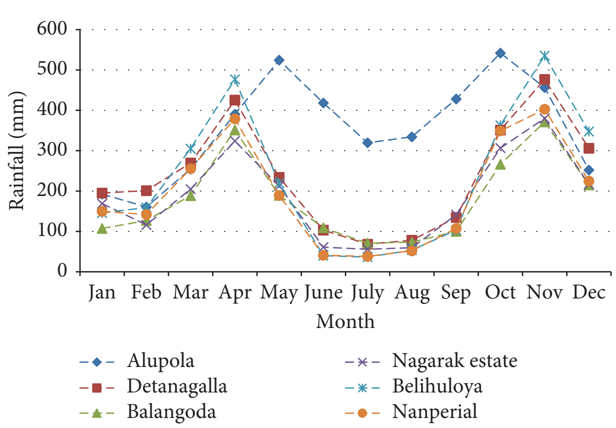

Figure 2: Monthly rainfall averaged over the period from 1993 to 2016.

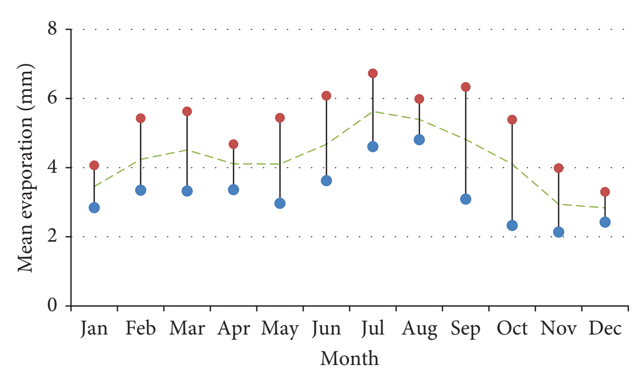

Figure 3: Monthly mean evaporation at the Samanalawewa reservoir site.

2.2.4. Power Generation Data. The annual power generation and its variation (from year 1993 – 2019) can be clearly seen from Figure 5. It can be traced that power generation has dropped sharply to 152 GWh in 1996, and since then, similar declines have occurred after every 5-6 years in 2002, 2007, 2012, and 2017 compared to the years around them. Similarly, the power generation has shown local maxima after every 5 years since 1993, and these maxima have occurred immediately after the years with local minima except in 1998.

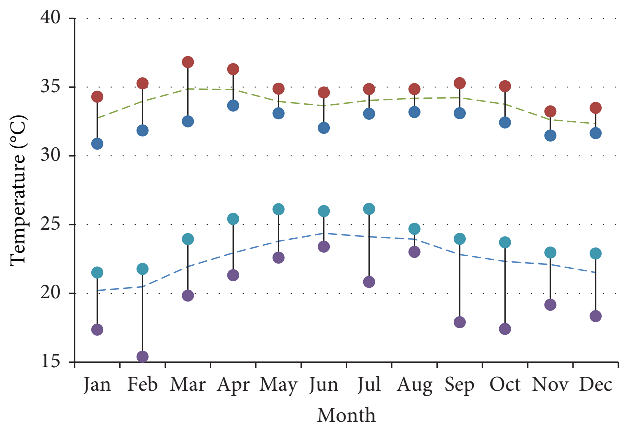

Figure 4: Monthly mean maximum and minimum temperatures.

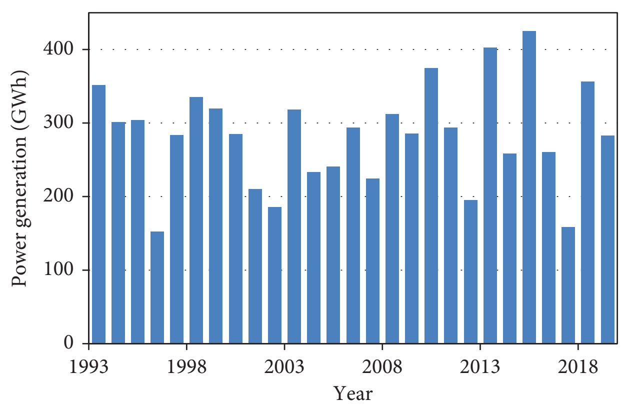

Figure 5: Annual power generation at the Samanalawewa power plant.

The minimum power generation (1.1 GWh) during the whole study period was found in November 2016. The associated rainfall during the preceding months of the same year was compiled with its November values at the six locations in Table 2 along with the power generated. This table shows that, except at Alupola, the rainfall has drastically decreased at other locations during the 4 month period from June to September, before picking up in October and reaching much higher values in November. Although power was generated uninterrupted, the effect of low rainfall has reflected through the nominal power outputs during September to November. It can also be understood that the rainfall experienced in November is comparable with the corresponding average values at each location presented in Figure 1, and that it has not created any positive impact on the power generated during the same month at the Samanalawewa power plant.

Furthermore, the monthly power generation averaged over the study period (1993–2019) was considered along with its maximum and minimum, shown in Figure 6. A detailed examination into data revealed that the maximum monthly power generation of 80.7 GWh was reported in January 1998, subsequent to a much higher rainfall since September 1997, e.g., a monthly rainfall over 340 mm at Alupola and Detanagalla. Moreover, Figure 6 shows the highest power generation during the two periods: April-May and November-January, which fall soon after the two months with the heaviest rainfall, April and November, indicated by the peaks in Figure 2. Therefore, it is evident that the rainfall of a particular month does not affect the power generation of the same month at Samanalawewa, which can justify the use of quarterly rainfall data for modelling instead of monthly data in this research.

3. Regression Techniques and Methodology

The hydropower generation at Samanalawewa from the year 1993 to 2019 was modelled in two time scales of monthly and quarterly data. Regression-based models were first developed by applying Gaussian process regression (GPR), support vector regression (SVR), multiple linear regression (MLR), and power regression (PR) to express the hydropower as a function of the catchment rainfall in monthly and quarterly scales. Then, another set of models was developed by applying the same techniques on multiple weather indices, viz., rainfall, mean reservoir evaporation, and mean minimum and maximum reservoir temperatures. Three options were considered based on the formation of quarterly data, such that Option 1 comprises of the grouping of months: Jan-Mar, Apr-Jun, Jul-Sep, and Oct-Dec, while Option 2 comprises of Feb-Apr, May-Jul, Aug-Oct, and Nov-Jan grouping. Option 3 included the clustering of months: Mar-May, Jun-Aug, Sep-Nov, and Dec-Feb. The models developed were then tested using the performance indicators given in equations (8)–(12) to understand the performance of the regression models.

The machine learning based models (SVR and GPR) were developed in the MATLAB environment (version 9.4.0.813654-R2018a), while the statistical models (MLR and PR) were developed by programming in the *R* software (R 4.0.3).

3.1. Support Vector Regression

3.1. Support Vector Regression. Support vector regressions (SVRs) are supervised machine learning models based on a regression algorithm that can deal with nonlinear data for prediction. It is highlighted due to its robustness and high prediction accuracy in the presence of dimensionality of the input space [14]. The training and testing data used in SVR are assumed to be independent and identically distributed having an unknown probability function. SVR develops a linear hyperplane that transforms multidimensional input vectors (weather indices) into output values (power generation), which are then used to predict future output values. For linear function f, a set of n number of data points $P = (x_i, y_i)$, where x_i is the input vector of a data point i and y_i is its actual value, the hyperplane $f(x)$ is given as follows [15]:

$$f(x) = wx_i + b, \tag{1}$$

where w is the slope and b is the intercept. For nonlinear relations, a map φ that translates x_i into a higher-dimensional feature space needs is defined. Then, w becomes a function of $\varphi(x_i)$, and the Kernel function is defined as a product as follows:

Table 2: Power generation and the rainfall received from June to November of 2016.

Month	Power (GWh)	Rainfall (mm) Alupola (RF_1)	Detanagalla (RF_2)	Balangoda (RF_3)	Nagarak Estate (RF_4)	Belihuloya (RF_5)	Nanperial (RF_6)
Jun 2016	33.4	236	26	61	18	8	18
Jul 2016	13.5	148	37	29	39	49	40
Aug 2016	13.4	241	8	19	14	19	14
Sep 2016	2.9	220	3	17	6	0	6
Oct 2016	2.5	581	93	131	100	77	102
Nov 2016	1.1	591	350	419	349	518	358

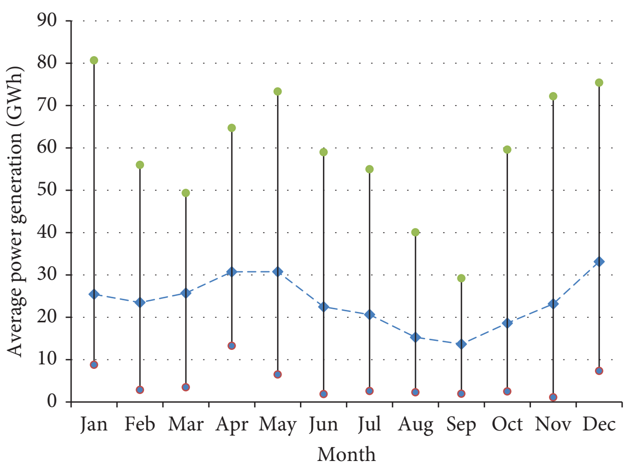

Figure 6: Monthly power generation averaged over the period from 1993 to 2019.

$$k(x_i, x) = \phi(x_i)\phi(x). \tag{2}$$

In this research, 5-fold crossvalidation was applied using 4 folds for training and the other fold for evaluation. It was repeated 5 times, using one different fold for evaluation each time. SVR-based prediction models were developed by applying Kernel functions of linear, quadratic, cubic, fine Gaussian, medium Gaussian, and coarse Gaussian, and the model that gives the lowest RMSE was selected for further analysis.

3.2. Gaussian Process Regression. Gaussian distribution is defined by its mean and the standard deviation, characterized by a symmetrical curve about the mean that coincides with the mode and the median. In statistical analysis, a Gaussian process is a stochastic process with every finite collection of random variables having a multivariate normal distribution [16]. Gaussian process regression (GPR) is nonparametric and useful in dealing with small datasets. Another advantage is its capacity to address uncertainty measurements of the predictions. A Gaussian process is denoted as follows [17]:

$$f(x) = \mathrm{GP}(m(x), k(x, x')), \tag{3}$$

where $m(x)$ and $k(x, x')$ are the mean function and the covariance function, respectively. The mean function $m(x)$ is the expectation of the function $f(x)$ at the point x, and the covariance function is a measure of the confidence level for $m(x)$. In this research, GPR-based models were developed by applying Kernel functions of rational quadratic, exponential, squared exponential, and Matern 5/2, and the model with the lowest RMSE was selected for further analysis.

3.3. Multiple Linear Regression. Multiple linear regression (MLR) assumes a linear relationship among the independent and dependent variables. Therefore, the best fit is described by a straight line of the relationship wherein the data are assumed to be normally distributed [18]. The general mathematical formula of the MLR model for n number of independent variables is written as follows [19]:

$$y = \beta_0 + \beta_1 x_1 + \beta_2 x_2 + \cdots + \beta_i x_i + \cdots + \beta_n x_n + \varepsilon, \tag{4}$$

where y is the dependent variable (power generation), β_0 is the intercept on the y axis, β_i is the slope coefficient of the i$^{\text{th}}$ input variable x_i, and ε is the model error.

3.4. Power Regression. Power regression (PR) develops a power relationship among the variables. The nonlinearity of data was considered in PR, which modelled the power generation proportional to the product of powers of the independent variables as follows [20–22]:

$$y = a x_1^b x_2^c \cdots x_n^p, \tag{5}$$

where n is the number of observations and $a, b, c, \ldots, p$ are constants.

3.5. Correlation Coefficient. Pearson's and Spearman's correlation coefficients were used to assess the collinearity among each pair of input and output variables. Monthly and quarterly data were used to determine the correlation coefficient.

Pearson's correlation coefficient is the most commonly used test statistic for measuring the linear dependency of two normally distributed random variables as it takes both variance and the covariance into account [23]. It indicates both the degree and the direction of the association, if any. Pearson's correlation coefficient (R_p) of two random variables X and Y is mathematically presented as follows [24]:

$$R_P = \frac{\text{covariance}(X, Y)}{\sqrt{\text{variance}(X)}\sqrt{\text{variance}(Y)}} = \frac{\sum_{i=1}^{N}(x_i - \overline{x})(y_i - \overline{y})}{\sqrt{\sum_{i=1}^{N}(x_i - \overline{x})^2 \sum_{i=1}^{N}(y_i - \overline{y})^2}}, \quad (6)$$

where $-1 \leq R_P \leq +1$. The values of R_P closer to ±1 are the evidence for strong associations, which should be reflected on the scatter plot between the two variables with close congregation of points around the line of the best fit. The intervals [±0.66, ±1], [±0.33, ±0.65], and [±0.32, 0] of R_P are considered as strong, medium, and low degree correlations, respectively.

Spearman's correlation coefficient may be viewed as the nonparametric counterpart of Pearson's correlation coefficient for nonlinear data, which also measures both the strength and direction of the two variables [25]. Its value also varies between −1 and +1 having a similar interpretation as for Pearson's correlation coefficient. The mathematical form of Spearman's correlation coefficient (r_s) is defined as follows when it is applied to n pairs of rank variables, and the ranks are distinct integers,

$$r_s = 1 - \frac{6\sum d_i^2}{n\left(n^2 - 1\right)}, \quad (7)$$

where d_i is the difference between the ranks of the two observations.

3.6. Evaluation Criteria of Developed Models. The following statistical measures: the correlation coefficient (R), mean absolute percentage error (MAPE), ratio of the root mean square error (RMSE) to the standard deviation of the measured data (RSR), BIAS, and the Nash number were used to evaluate the dexterity of each model developed in the present study based on the mathematical formula indicated in the following equations:

$$\text{correlation coefficient; } R = \frac{\sum_{i=1}^{N}(x_i - \overline{x})(y_i - \overline{y})}{\sqrt{\sum_{i=1}^{N}(x_i - \overline{x})^2 \sum_{i=1}^{N}(y_i - \overline{y})^2}}, \quad (8)$$

$$\text{MAPE} = \frac{1}{N}\sum_{i=1}^{N}\left|\frac{x_i - y_i}{x_i}\right| \times 100, \quad (9)$$

$$\text{RSR} = \frac{\sqrt{\text{MSE}}}{\sigma_x}, \quad (10)$$

$$\text{BIAS} = \frac{\sum_{i=1}^{N}(y_i - x_i)}{N}, \quad (11)$$

$$\text{Nash number} = 1 - \left[\frac{\sum_{i-1}^{N}(x_i - y_i)^2}{\sum_{i-1}^{N}(x_i - \overline{x})^2}\right], \quad (12)$$

where x_i is the actual power generation, y_i is the predicted power generation, $\overline{x}$ and $\overline{y}$ are their means, N is the number of data values, and σ_x is the standard deviation of actual power generation. The values of MAPE and RSR closer to zero and R the Nash number closer to 1 imply more accurate models for the prediction of power generation. A zero BIAS means accurate models, whereas its negative and positive values would indicate underestimation and overestimation, respectively.

4. Results and Discussion

The following subsections present the results obtained from the regression analysis for hydropower generation at the Samanalawewa hydropower plant based on the catchment rainfall, reservoir evaporation, and temperature. The analysis was carried out using the regression models described in the previous section.

4.1. Models Developed Based on Monthly Data. Correlations between the hydropower generation and the monthly rainfall of six rain gauges in the catchment area are presented in Table 3. Results clearly show that there is very little correlation between the power generation and rainfall at monthly scale.

This observation is further consolidated by the performance (R) of the regression models in the monthly scale, shown in Table 4. Out of the SVR models developed by applying six types of kernels, the fine Gaussian SVR demonstrated the best performance. Exponential GPR is the most accurate among the GPR models developed by applying four kernels. The results revealed that none of the regression-based prediction models is accurate when the monthly rainfall at the catchment area is used as the input variables.

Based on these results, it can be clearly concluded that the monthly scale is not appropriate for regression analysis in compliance with the observations drawn from Table 2. Therefore, quarterly models were developed by using quarterly rainfall data as input variables.

4.2. Quarterly Models Developed Based on Rainfall Data. The following results presented in Table 5 and Figure 7 are based on the models developed with respect to the quarterly rainfall data. Figure 7 shows the relationship between the observed power generation and the predicted power generation produced by the regression-based prediction models.

Based on the deviations of the predictions, it can be clearly seen that the machine learning models (Figures 7(a) and 7(b)) outperform the statistical models (Figures 7(c) and 7(d)). Fine Gaussian SVR outperformed the other five types of SVR-based models, while the rational quadratic GPR was the most accurate among the GPR-based models. Power generation values predicted by the SVR and GPR models are closer to the reality, which correspond to the coefficient of correlation reaching 1 with least error in

Table 3: Coefficient of correlation between hydropower generation and monthly rainfall.

Rainfall of rain gauges	RF_1	RF_2	RF_3	RF_4	RF_5	RF_6
Coefficient of correlation	0.07	0.25	0.24	0.17	0.16	0.11

Table 4: Performance of the prediction models for monthly rainfall data.

Regression technique	SVR	GPR	MLR	PR
R	0.25	0.28	0.29	0.39

Table 5: Performance of the regression models based on quarterly rainfall.

Statistical measure (performance indicator)	Regression technique			
	SVR	GPR	MLR	PR
R	0.86	0.95	0.49	0.61
MAPE (%)	20.2	7.0	60.3	39.3
BIAS	−0.7	0.4	7.1	−4.9
Nash	0.7	0.9	0.2	0.2
RSR	0.5	0.3	0.9	0.9

terms of MAPE, BIAS, Nash number, and the RSR (Table 5). The excellence of GPR compared to SVR is evident from the highest *R* and Nash number, least MAPE and RSR, and a smaller BIAS.

Moreover, the coefficients of correlation are much higher in Table 5 compared to those in Table 4, which reinforces the appropriateness of using quarterly data instead of the monthly data. Among the four techniques, the models based on SVR and GPR show much better performance compared to the other two models. The MLR model has the lowest performance as indicated by the performance evaluators of *R* and the MAPE in particular. Furthermore, it has the highest BIAS and RSR as well. Therefore, compared to other regression models, the GPR model can be recommended as an outstanding technique.

4.3. Quarterly Models Developed Based on Four Meteorological Factors. Table 6 summarizes the correlation coefficients generated by all the models for the three seasonal options tested on quarterly basis with respect to the four climatic variables. In all three seasonal options, fine Gaussian SVR was the best among SVR-based models. Rational quadratic outperforms other GPR kernels in the first and second seasonal options, while Matern 5/2 was the best GPR in the third seasonal option. As was seen in Table 5, the GPR model has outperformed the other regression models. Furthermore, equally better performance can be seen between the GPR and SVR models. Similarly close results are observed between these models irrespective of the three seasonal clusters used in the quarterly analysis. In addition, the correlation coefficients suggest that the MLR and PR are not the best regression techniques to predict the hydropower generation in the Samanalawewa hydropower plant in Sri Lanka.

Table 7 presents Pearson's and Spearman's correlation coefficients between the power generation and each catchment rainfall of the six rain gauges and among the paired rain gauges. According to the interpretation of the size of these coefficients introduced in Section 3.5, it can be noticed that very strong pairwise correlations exist between the rainfall received in the catchment areas of Balangoda (RF_3), Nagarak Estate (RF_4), Belihuloya (RF_5), and Nanperial (RF_6), respectively. Moderate correlations appear between the power generation and each of the five rain gauges except at Alupola (RF_1). The only exception with the weakest correlation between rainfall and the power generation is reported from Alupola.

Figure 8 illustrates the relationship between the predicted and the observed power generation. The strong linear relationships between the observed and predicted values in Figures 8(a) and 8(b) indicate that machine learning (SVR and GPR) models forecast the hydropower generation with remarkable accuracy (more than 87%). However, the predicted power generation for the MLR and PR regression models is scattered around the line of best fit as shown in Figures 8(c) and 8(d).

The results shown in Table 6 and Figure 8 are further verified by the model performance indicators in Table 8, which arise from the four regression models applied for Option 1. The GPR regression model presents the best results with the lowest errors and the highest correlation coefficient. Therefore, it can be concluded that the GPR regression model is a better regression model compared to others to predict the hydropower generation in the Samanalawewa hydropower plant.

Similar observations and findings could be seen in the other two options too (which are not shown here). Therefore, the superiority of the GPR model could be generalized for the power generation at Samanalawewa irrespective of the seasonal options.

4.4. Comparison of Similar Research. Table 9 presents a summary of some related work in the literature on the prediction of hydropower generation based on climatic data and using different modelling techniques in several countries. Most of the research studies are based on ANNs. A major drawback of ANNs was discussed in the introduction section of this paper. Even though they showcased better results, the black box environment in analysis leads to less information of the relationship. Some other methods like stepwise regression have also been used to predict the hydropower development. However, in most of these studies, only one statistical measure, i.e., correlation coefficient, was used to evaluate the prediction accuracy. Therefore, it could be analytically proved with evidence that out of the four prediction models developed in this study, the GPR has shown excellent performance and even outperformed all the models cited here. In particular, in the previous study conducted on the Samanalawewa hydropower generation, only the ANN was applied, and the performance was evaluated only in terms of the correlation coefficient and the MSE [6]. All the ANN-based prediction models were found

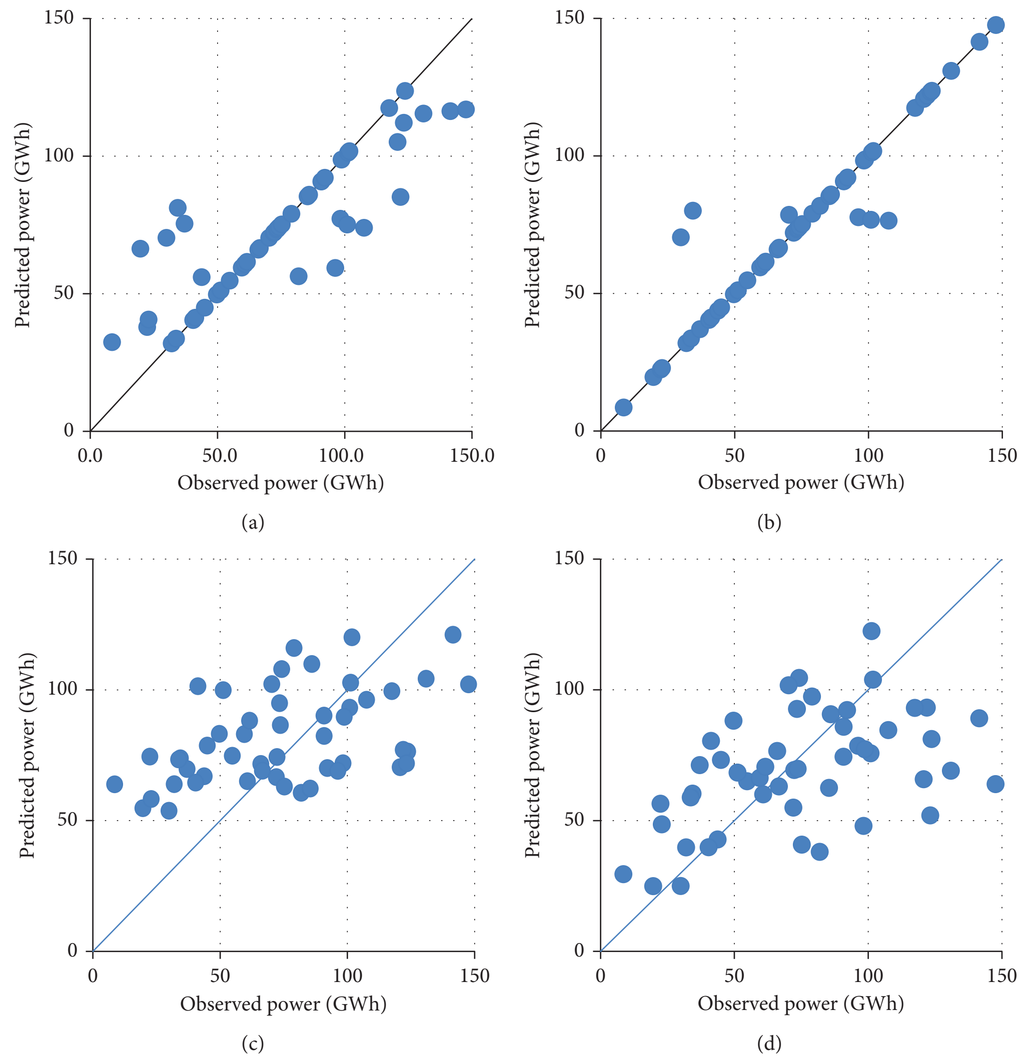

Figure 7: Predicted power generation against the observed power generation. (a) For SVR. (b) For GPR. (c) For MLR. (d) For PR.

Table 6: Correlation coefficients for the regression models based on quarterly climatic data.

	Regression technique			
	SVR	GPR	MLR	PR
Option 1	0.87	0.92	0.60	0.67
Option 2	0.87	0.91	0.44	0.45
Option 3	0.91	0.94	0.44	0.45

Table 7: Matrix of Pearson's (R) and Spearman's (r_s) correlation coefficients.

Power	1						
RF_1	$R = 0.10$ $r_s = 0.11$	1					
RF_2	$R = 0.35$ $r_s = 0.39$	$R = 0.38$ $r_s = 0.39$	1				
RF_3	$R = 0.33$ $r_s = 0.35$	$R = 0.50$ $r_s = 0.50$	$R = 0.83$ $r_s = 0.90$	1			
RF_4	$R = 0.45$ $r_s = 0.46$	$R = 0.36$ $r_s = 0.34$	$R = 0.85$ $r_s = 0.86$	$R = 0.85$ $r_s = 0.87$	1		
RF_5	$R = 0.35$ $r_s = 0.39$	$R = 0.38$ $r_s = 0.40$	$R = 0.90$ $r_s = 0.94$	$R = 0.94$ $r_s = 0.94$	$R = 0.90$ $r_s = 0.90$	1	
RF_6	$R = 0.34$ $r_s = 0.38$	$R = 0.28$ $r_s = 0.30$	$R = 0.88$ $r_s = 0.89$	$R = 0.80$ $r_s = 0.85$	$R = 0.90$ $r_s = 0.91$	$R = 0.88$ $r_s = 0.91$	1
	Power	RF_1	RF_2	RF_3	RF_4	RF_5	RF_6

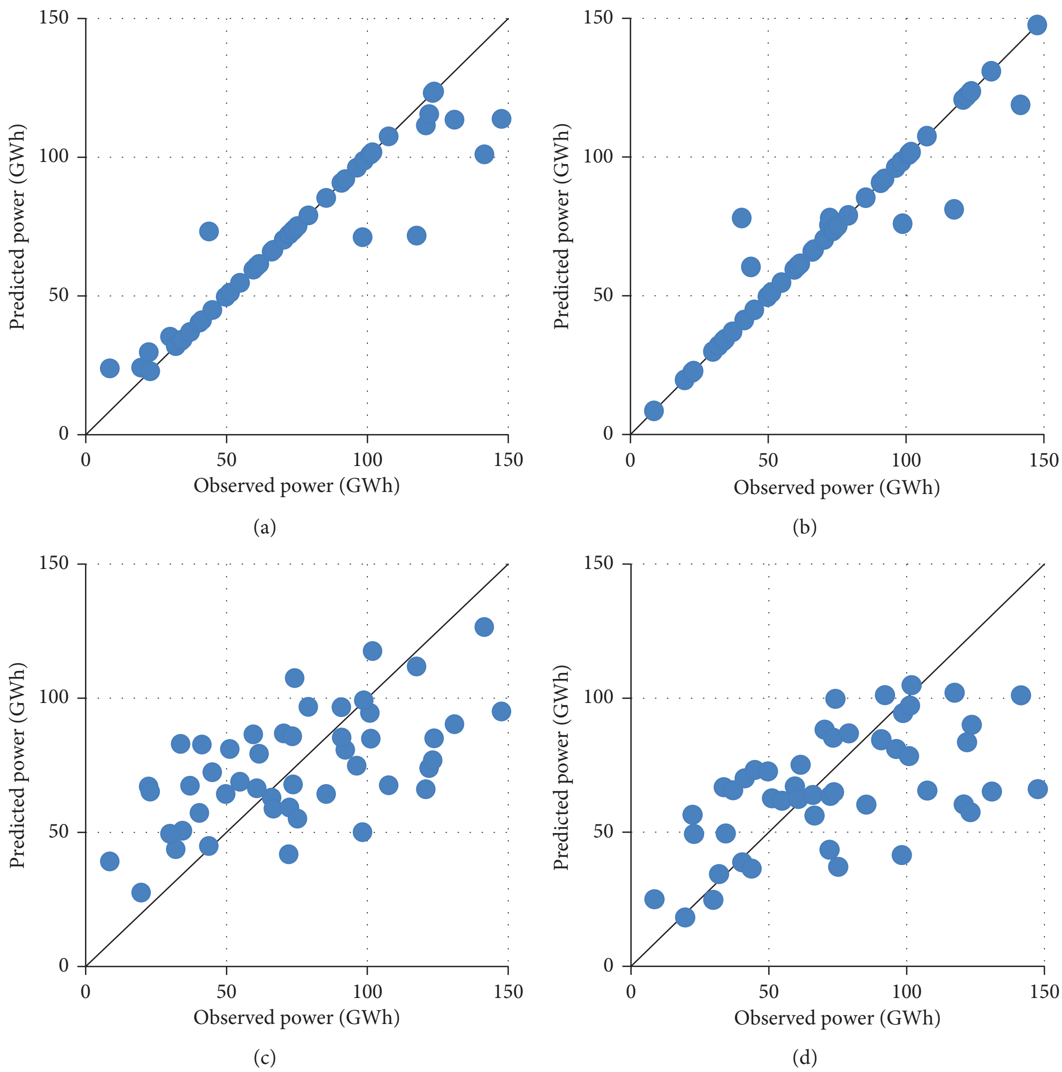

FIGURE 8: Predicted power generation vs. the observed power generation. (a) For SVR, (b) For GPR, (c) For MLR, (d) For PR.

TABLE 8: Performance of the models based on quarterly climate data for option 1.

Statistical measure (performance indicator)	Regression technique			
	SVR	GPR	MLR	PR
R	0.87	0.92	0.60	0.67
MAPE (%)	9.7	4.5	46.1	35.7
BIAS	−2.5	−0.4	−0.01	−7.1
Nash	0.9	0.9	0.4	0.3
RSR	0.4	0.3	0.8	0.8

TABLE 9: Comparison of previous related studies.

Ref	Country of study	Input variables	Modeling technique	Performance of the models
[3]	Ghana	Temperature and rainfall	Statistical analysis	—
			ANN (LM)	$R = 0.86$ $MSE = 1.03 \times 10^6$
[6]	Sri Lanka	Rainfall	ANN (BR)	$R = 0.73$ $MSE = 8.9 \times 10^3$
			ANN (SCG)	$R = 0.76$ $MSE = 7.42 \times 10^5$

Table 9: Continued.

Ref	Country of study	Input variables	Modeling technique	Performance of the models
[7]	Nigeria	Evaporation losses, reservoir inflow, storage, reservoir elevation, turbine release, net generating head, plant use coefficient, tail race level	ANN	$R = 0.89$
[8]	Brazil	Rainfall at seven subbasins	Group method of data handling (GMDH)	$R = 0.90$ MAE = 443 MAPE = 12.34%
			ANN (BR)	$R = 0.88$ MAE = 450 MAPE = 12.41%
			ANN (LM)	$R = 0.83$ MAE = 593 MAPE = 17%
[9]	Ghana	Rainfall, ENSO, lake level elevation, and net lake inflow	Stepwise multiple regression	$R^2 = 0.753$ Adjusted $R^2 = 0\ .742$

less accurate than the GPR-based model presented in this paper. In this sense, the scientific contribution of the present paper is well justified.

5. Conclusions

The paper presented highly accurate models for the prediction of hydropower generation by using machine learning techniques. Particularly, the GPR-based prediction models outperformed the other techniques used in this research, as well as in similar studies conducted on hydropower plants located in other countries. Therefore, when the future rainfall of the catchment area is known by forecast, the power generation at the Samanalawewa hydropower station can be predicted accurately. It could also be concluded that the monthly rainfall is not reflected through the power generated during the same month at Samanalawewa. The lack of correlation between the hydropower generation and the monthly rainfall of rain gauges in the catchment area clearly indicated that monthly data are not the best for forecasting the power generation, rather it is the quarterly rainfall that produced the most accurate predictions with high correlation.

The prediction of power generation at this major power plant in Sri Lanka will certainly provide useful information, not only for the energy authorities of the country but also for the policy makers, investors, and the government in ensuring uninterrupted power supply through an environmentally friendly renewable source at affordable cost to the consumers. The climate models can effectively be used in forecasting the climate patterns for future years under different representative concentration pathways (*RCP2.6, RCP4.5, RCP6, and RCP8.5*). These predicted climate data can be used in the prediction models developed in this study to forecast the hydropower generation at the Samanalawewa hydropower plant in future years (in 2030 to 2099). Thus, the findings of this research would be highly useful for the future planning processes.

Data Availability

The climatic data and the analysis data are available from the corresponding author upon request.

Disclosure

The research was carried out at the Wayamba University of Sri Lanka and the Sri Lanka Institute of Information Technology environments.

Conflicts of Interest

The authors declare that there are no conflicts of interest.

Acknowledgments

The authors would like to acknowledge the support from the Ceylon Electricity Board, Sri Lanka, and the support by Dr. Kamal Laksiri in providing the Samanalawewa Hydropower generation data. In addition, the authors would like to thank Ms. Imiya Chathurinika for creating the catchment drawing for the Samanalwewa catchment.

References

[1] G. Dabare, M. B. Gunathilake, N. Miguntanna, K. Laksiri, and U. Rathnayake, "Climate variation and hydropower generation in samanalawewa hydropower scheme, Sri Lanka," *Engineer: Journal of the Institution of Engineers, Sri Lanka*, vol. 53, no. 3, pp. 19–25, 2020.

[2] Y. Suleiman and L. Ifabiyi, "The role of rainfall variability in reservoir storage management at Shiroro Hydropower Dam, Nigeria," *Momona Ethiopian Journal of Science*, vol. 7, no. 1, pp. 55–63, 2015.

[3] A. Kabo-Bah, C. Diji, K. Nokoe, Y. Mulugetta, D. Obeng-Ofori, and K. Akpoti, "Multiyear rainfall and temperature trends in the Volta river basin and their potential impact on hydropower generation in Ghana," *Climate*, vol. 4, no. 4, p. 49, 2016.

[4] B. Khaniya, C. Karunanayake, M. B. Gunathilake, and U. Rathnayake, "Projection of future hydropower generation in Samanalawewa power plant, Sri Lanka," *Mathematical Problems in Engineering*, vol. 2020, Article ID 8862067, 11 pages, 2020.

[5] M. Beheshti, A. Heidari, and B. Saghafian, "Susceptibility of hydropower generation to climate change: Karun III Dam case study," *Water*, vol. 11, no. 5, Article ID 1025, 2019.

[6] A. Perera and U. Rathnayake, "Relationships between hydropower generation and rainfall-gauged and ungauged catchments from Sri Lanka," *Mathematical Problems in Engineering*, vol. 2020, Article ID 9650251, 8 pages, 2020.
[7] T. S. Abdulkadir, A. W. Salami, A. R. Anwar, and A. G. Kareem, "Modelling of hydropower reservoir variables for energy generation: neural network approach," *Ethiopian Journal of Environmental Studies and Management*, vol. 6, no. 3, pp. 310–316, 2013.
[8] M. N. G. Lopes, B. R. P. da Rocha, A. C. Vieira, J. A. S. de Sá, P. A. M. Rolim, and A. G. da Silva, "Artificial neural networks approaches for predicting the potential for hydropower generation: A case study for Amazon region," *Journal of Intelligent & Fuzzy Systems*, vol. 36, no. 6, pp. 5757–5772, 2019.
[9] S. A. Boadi and K. Owusu, "Impact of climate change and variability on hydropower in Ghana," *African Geographical Review*, vol. 38, no. 1, pp. 19–31, 2019.
[10] D. Carless and P. G. Whitehead, "The potential impacts of climate change on hydropower generation in Mid Wales," *Hydrology Research*, vol. 44, no. 3, pp. 495–505, 2013.
[11] B. Khaniya, H. G. Priyantha, N. Baduge, H. M. Azamathulla, and U. Rathnayake, "Impact of climate variability on hydropower generation: A case study from Sri Lanka," *ISH Journal of Hydraulic Engineering*, vol. 26, no. 3, pp. 301–309, 2020.
[12] K. Laksiri, "A modern addition—uncovering Samanalawewa," *International Water Power and Dam Construction*, Archived from the original on 2010-01-09. Retrieved 2009-06-27, 2004.
[13] K.-H. Nagel, "Limits of the geological predictions constructing the Samanalawewa pressure tunnel, Sri Lanka," *Bulletin of the International Association of Engineering Geology*, Springer, vol. 45, no. 1, , pp. 97–110, Berlin, Germany, 1992.
[14] M. Awad and R. Khanna, *Efficient Learning Machines: Theories, Concepts, and Applications for Engineers and System Designers*, Springer nature, Basingstoke, UK, 2015.
[15] M. Wauters and M. Vanhoucke, "Support vector machine regression for project control forecasting," *Automation in Construction*, vol. 47, pp. 92–106, 2014.
[16] D. Kong, Y. Chen, and N. Li, "Gaussian process regression for tool wear prediction," *Mechanical Systems and Signal Processing*, vol. 104, pp. 556–574, 2018.
[17] C. E. Rasmussen and C. K. I. Williams, *Gaussian Processes for Machine Learning*, The MIT Press, Cambridge, MA, USA, 2006.
[18] G. K. Uyanık and N. Güler, "A study on multiple linear regression analysis," *Procedia-Social and Behavioral Sciences*, vol. 106, pp. 234–240, 2013.
[19] M. Tranmer and M. Elliot, "Multiple linear regression," *The Cathie Marsh Centre for Census and Survey Research (CCSR)*, vol. 5, no. 5, pp. 1–5, 2008.
[20] R. G. Shepherd, "Regression analysis of river profiles," *The Journal Of Geology*, vol. 93, no. 3, pp. 377–384, 1985.
[21] S. d. Jong, B. M. Wise, and N. L. Ricker, "Canonical partial least squares and continuum power regression," *Journal Of Chemometrics*, vol. 15, no. 2, pp. 85–100, 2000.
[22] V. Gowariker, V. Thapliyal, R. Sarker, G. Mandal, and D. Sikka, "Parametric and power regression models: New approach to long range forecasting of monsoon rainfall in India," *Mausam*, vol. 40, no. 2, pp. 115–122, 1989.
[23] K. H. Zou, K. Tuncali, and S. G. Silverman, "Correlation and simple linear regression," *Radiology*, vol. 227, no. 3, pp. 617–628, 2003.
[24] D.-S. Lee, C.-S. Chang, and H.-N. Chang, "Analyses of the clustering coefficient and the Pearson degree correlation coefficient of chung's duplication model," *IEEE Transactions on Network Science and Engineering*, vol. 3, no. 3, pp. 117–131, 2016.
[25] J. H. Zar, "Spearman rank correlation," *Encyclopedia of Biostatistics*, Wiley, vol. 7Hoboken, NJ, USA, , 2005.